minerals

MDPI

Review

Core Spectral Technology in Sandstone-Type Uranium Deposits of Basins in Northern China: Applications and Challenges—A Review

Wenyi Wu, Mingsen Fan *, Pei Ni *, Junyi Pan, Yihan Lin, Zhe Chi and Junying Ding

State Key Laboratory of Critical Earth Material Cycling and Mineral Deposits, Institute of Geo-Fluids, School of Earth Sciences and Engineering, Nanjing University, Nanjing 210093, China; wenyi420@163.com (W.W.); pjynju2010@126.com (J.P.); 602025290010@smail.nju.edu.cn (Y.L.); dg1929001@smail.nju.edu.cn (Z.C.); jyding@nju.edu.cn (J.D.)

* Correspondence: fmsnju2016@163.com (M.F.); peini@nju.edu.cn (P.N.)

Abstract

Sandstone-type uranium deposits represent one of the most significant uranium deposit types in China, predominantly hosted in Meso-Cenozoic sedimentary basins in the northern part of the country. Due to characteristics such as deep burial of orebodies, fine grain size of ores, and strong heterogeneity, traditional geological logging methods have limitations in rapidly and accurately identifying alteration minerals and mineralization indicator information. Core spectral technology (wavelength range approximately 400–2500 nm), particularly short-wave infrared spectroscopy (SWIR, 1300–2500 nm), enables rapid, non-destructive, and quantitative extraction of alteration mineral information from drill cores. This provides robust technical support for reconstructing metallogenic environments, delineating oxidation–reduction zones, and prospecting and prediction in sandstone-type uranium deposits. This review systematically examines the spectral absorption characteristics and geological significance of key alteration minerals (e.g., clay minerals, carbonate minerals, iron oxides, and hydrocarbon substances) in sandstone-type uranium deposits. It elaborates on the current application status of core spectral technology in sandstone-type uranium exploration within typical basins in northern China, such as the Ordos, Songliao, Erlian, and Qaidam Basins. These applications include alteration mineral mapping, oxidation–reduction zone delineation, and metallogenic fluid tracing. Due to the unique characteristics of host rock lithology, alteration mineral assemblages, and fluid properties in sandstone-type uranium deposits, the application of this technology also faces certain challenges, such as difficulties in spectral interpretation and insufficient accuracy in quantitative inversion. Integrating this technique with multiple methods, including petrography and X-ray diffraction (XRD), will facilitate more effective applications in both metallogenic research and prospecting practices for sandstone-type uranium deposits in northern China.

Keywords: core spectral technology; short-wave infrared spectroscopy (SWIR); sandstone-type uranium deposit; alteration identity; basins in northern China

Academic Editor: Santanu Banerjee

Received: 20 March 2026
Revised: 25 April 2026
Accepted: 28 April 2026
Published: 30 April 2026

1. Introduction

Uranium resources are a critical strategic resource for national security and the development of clean energy. Sandstone-type uranium deposits, owing to their advantages such as large reserves, low cost, and relatively environmental friendliness, are among the world's

most important types of uranium deposits. With the progression of exploration efforts and the application of in situ leaching (ISL) technology, sandstone-type uranium deposits have also become the main exploration target in China, accounting for 72% of the country's total uranium production in 2021 (Figure 1) [1]. However, China's uranium resources are still relatively scarce, constituting only 4.38% of the world's total [2,3]. According to national development plans, domestic uranium resources are far from sufficient to meet developmental needs, resulting in a high dependence on foreign supplies. There is an urgent need to further strengthen investment in uranium exploration and discover more uranium resources. In recent years, China has achieved a series of major breakthroughs in the search for in situ leachable sandstone-type uranium deposits within Meso-Cenozoic sedimentary basins in the northern part of the country. Notably, a number of significant sandstone-type uranium deposits and metallogenic potential areas have been identified in basins such as the Ordos, Songliao, Erlian, and Qaidam Basins (Figure 1) [4–8].

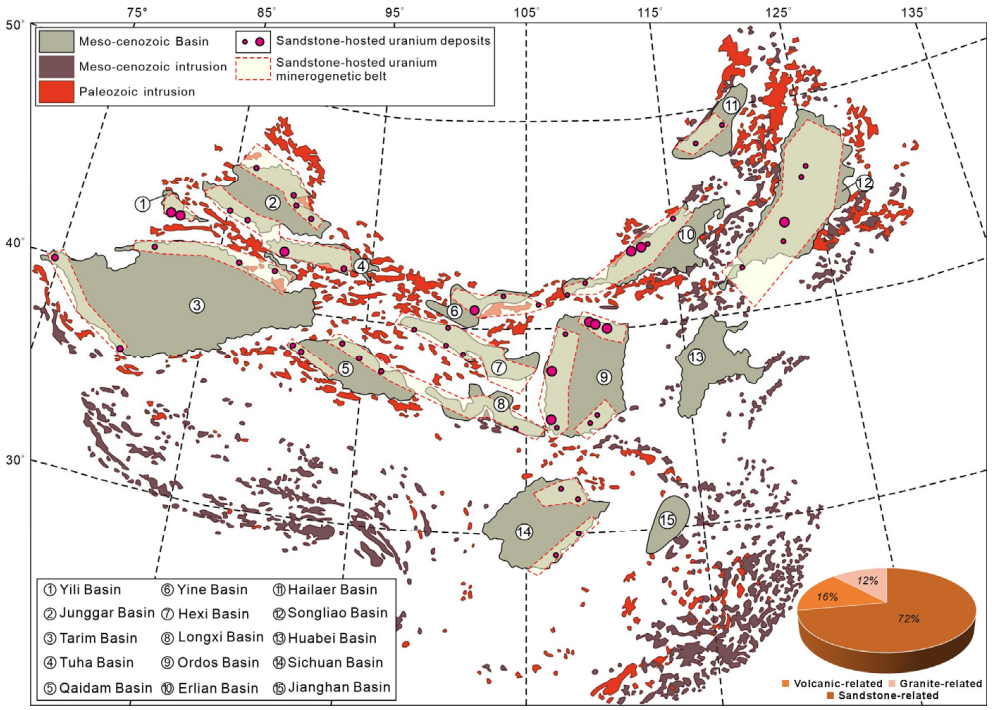

Figure 1. Distribution map of sandstone-type uranium deposits in the Meso-Cenozoic basins, North China (modified after [7,9]).

Sandstone-type uranium deposits are formed by the enrichment of U^{4+} when U^{6+}-bearing fluids migrate to the oxidation–reduction transition zone within sandstones and are reduced by reductants such as pyrite, organic matter, or hydrocarbon fluids [10]. During fluid–rock interaction, minerals that may record information about the mineralizing fluids are formed [11]. Alteration minerals are important components of the uranium-hosting sandstones in these deposits, and previous studies have extensively investigated them [8,12–17]. It has been established that alteration is widespread in sandstone-type uranium deposits within basins of northern China. The main alteration types include pyritization, hematitization, limonitization, chloritization, calcitization, bituminization, and kaolinization (Figures 2 and 3), and the dominant alteration types vary among different basins (Figure 2). For example, in the Qaidam Basin, mineralization-related alterations in the Yuejin-II and Qigequan deposits are primarily chlorite, carbonate, pyrite, and illite (Figures 2 and 3A–E) [8,18]. In the Luhai uranium deposit of the Erlian Basin, the primary mineralization-related alteration is kaolinite (Figure 2) [19]. In the Jingchuan uranium deposit of the Ordos Basin, the main mineralization-related alterations are chlorite and

carbonate (Figures 2 and 3H) [7]. Due to their fine grain size and high specific surface area, these alteration minerals are extremely sensitive to changes in fluid physicochemical conditions (e.g., pH, Eh, temperature, salinity). Their types, assemblages, abundances, and spatial distribution patterns record the evolutionary history of diagenetic and mineralizing fluids, as well as the characteristics of the metallogenic environment [12,20]. Various scholars have leveraged this property, integrating alteration mineral types and assemblage patterns with geological processes such as sediment provenance, paleoclimate, tectonic setting, and geochemical environmental changes to analyze the diagenetic and metallogenic processes of sandstone-type uranium deposits [21–27]. Currently, research on alteration minerals in sandstone-type uranium deposits primarily relies on traditional methods such as visual core logging, microscopic petrographic analysis, and X-ray diffraction (XRD) analysis. Constrained by factors like sample quantity, individual identification capabilities, and analytical costs, obtaining macro-scale distribution information of alteration minerals is often difficult. This, in turn, limits research on fluid migration directions and distinguishing the effects of sedimentation-diagenesis from mineralization-related fluids in these deposit types [12].

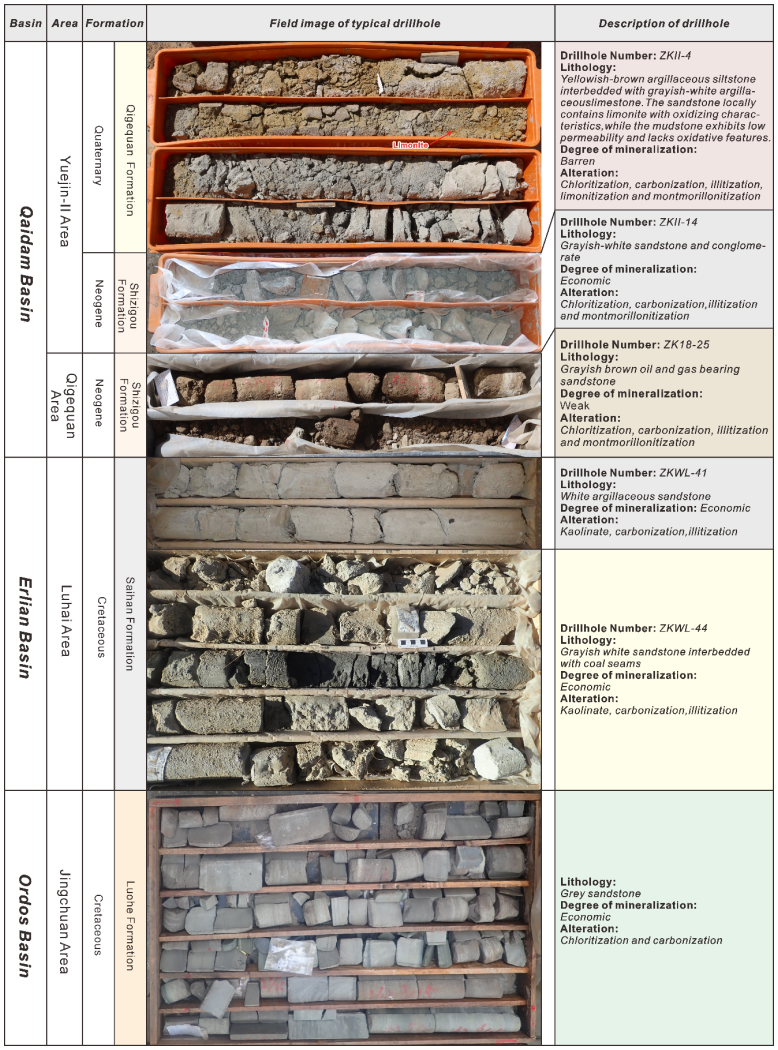

Figure 2. Representative drill core photographs from the Yuejin-II sandstone-type uranium deposit in the Qaidam Basin (from [8]), the Qigequan sandstone-type uranium deposit in the Qaidam Basin, the Luhai sandstone-type uranium deposit in the Erlian Basin, and the Jingchuan sandstone-type uranium deposit in the Ordos Basin (modified from [7]), illustrating the diversity of alteration across different basins.

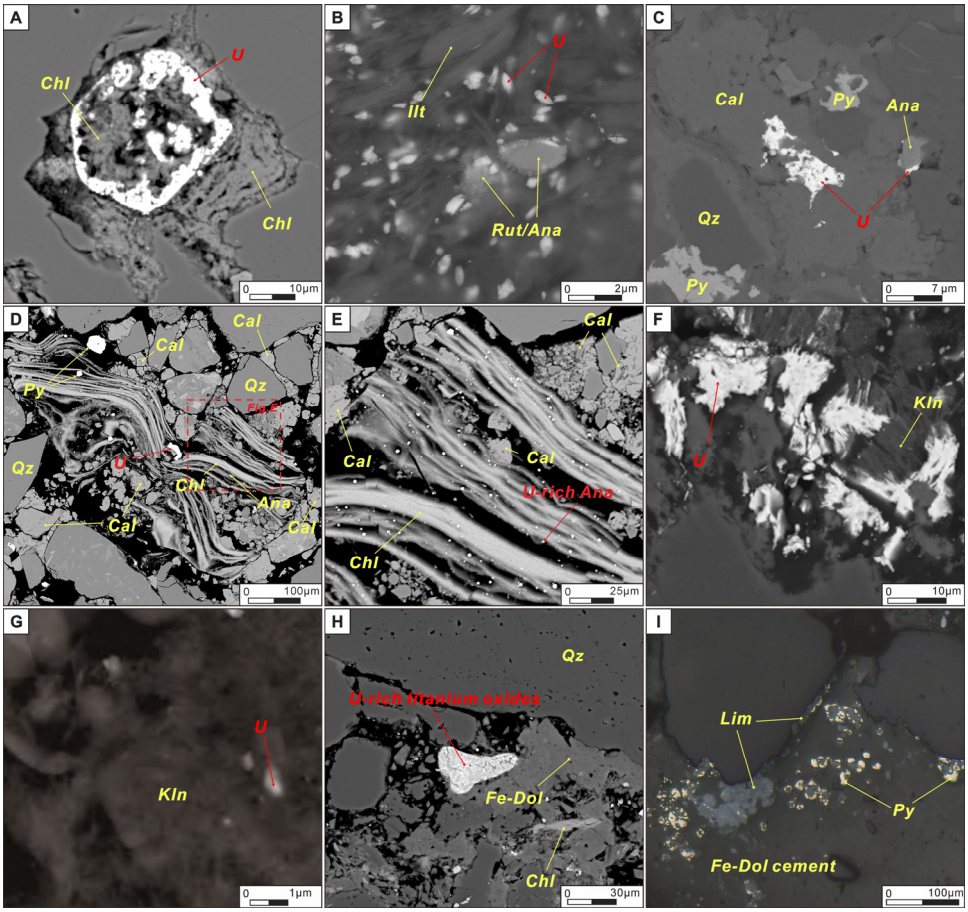

Figure 3. (**A**–**C**) Backscattered electron (BSE) images of alteration minerals associated with uranium minerals in the Qigequan sandstone-type uranium deposit. Qaidam Basin: (**A**) Chlorite intergrown with uranium minerals; (**B**) Illite intergrown with uranium minerals (modified from [18]); (**C**) Carbonate minerals and pyrite intergrown with uranium minerals (modified from [18]). (**D**,**E**) BSE images of alteration minerals (chlorite, carbonate) associated with uranium minerals in the Yuejin-II sandstone-type uranium deposit, Qaidam Basin (modified from [8]). (**F**) Scanning electron microscope (SEM) image of kaolinite associated with uranium minerals in the Qianjiadian sandstone-type uranium deposit, Songliao Basin (from [13]). (**G**) SEM image of kaolinite associated with uranium minerals in the Saihan Formation, Sangendalai Sag, Chuanjing Depression, Erlian Basin (from [17]). (**H**) BSE image of chlorite and carbonate minerals associated with uranium minerals in the Jingchuan sandstone-type uranium deposit, Ordos Basin (modified from [7]). (**I**) Limonite inclusions within Fe-bearing dolomite, an alteration mineral in the Jingchuan sandstone-type uranium deposit, Ordos Basin, PRL (modified from [7]). Abbreviations: Ana = anatase, Cal = calcite, Chl = chlorite, Ilt = illite, Py = pyrite, Qz = quartz, Rut = rutile, U = uranium minerals, Kln = kaolinite, Zrn = zircon, Xen = xenotime, Dol = dolomite, PRL = plane polarized reflected light.

Core spectral technology is a mapping technique that has been developed and gradually matured in recent years. Sandstone-type uranium deposits are often blind ore deposits, and their key prospecting geological information primarily relies on geological drilling for exposure. Therefore, drill core is of particular significance in sandstone-type uranium exploration [16]. Traditional manual core logging depends on the experience of geologists and suffers from issues such as strong subjectivity, low efficiency, and difficulty in identifying subtle alteration minerals. The advent of core spectral technology provides an excellent solution to this problem, enabling rapid, efficient, and relatively accurate extraction of alteration mineral information from sandstone-type uranium cores. This technology identifies and semi-quantitatively extracts mineral information from cores based on their diagnostic spectral features at specific wavelengths, thereby guiding sandstone-type uranium

exploration [28]. Currently, this technology primarily utilizes the visible-to-near-infrared and short-wave infrared spectral range (approximately 0.4–2.5 μm). The visible-to-near-infrared region (0.4–1.3 μm) can effectively identify electronic transition processes of certain transition metal ions (Fe^{3+}, Cr^{3+}, Mn^{3+}, rare earth elements, etc.), typically exhibiting broad absorption bands. The short-wave infrared region (1.3–2.5 μm) mainly detects overtones and combinations of molecular vibrations in hydrous and hydroxyl-bearing minerals (clay minerals, carbonates, some hydrated sulfates), characterized by relatively narrow absorption bands [29,30]. Notably, the sensitivity of the short-wave infrared region to hydroxyl-bearing, hydrous minerals, and hydrocarbon substances aligns perfectly with the research needs for major alteration types like clay alteration and carbonatization in sandstone-type uranium deposits. Analyzing core spectral data with specialized software allows for effective interpretation and semi-quantitative estimation of information such as organic carbon, total clay content, kaolinite content, and total iron content in target horizons. This, in turn, supports the screening of favorable horizons and the detailed analysis of fluid alteration and uranium mineralization processes [12,31]. Overall, core spectral technology offers significant advantages in analyzing alteration minerals (e.g., kaolinite, illite, chlorite, carbonate) due to its speed and efficiency, coupled with its portability, low cost, and non-destructive nature, making it an ideal tool for alteration identification. Coupled with the widespread occurrence of alteration and its diversity across different basins in northern China (Figure 2), this provides a strong rationale for the application of this technology and is a key motivation for this review to synthesize these application practices.

Although core spectral technology has established relatively mature prospecting criteria and application systems in magmatic–hydrothermal deposits [32–35], sandstone-type uranium deposits differ fundamentally from magmatic–hydrothermal systems in terms of host rock lithology, alteration mineral assemblages, and fluid properties. The former is characterized by complex host rock lithologies (interbedded sandstone and mudstone), alteration minerals that can be easily confused with sedimentary–diagenetic backgrounds, and low-temperature oxidation–reduction fluid systems. These differences necessitate the establishment of a specialized evaluation system and workflow when applying this technology to sandstone-type uranium deposits. In recent years, Chinese scholars have conducted extensive core spectral research in basins such as the Ordos, Songliao, Erlian, and Qaidam, accumulating a number of typical case studies and important insights. However, systematic synthesis and review of these research findings are currently lacking.

Based on the above background, this review aims to: (1) systematically summarize the fundamental principles of core spectral technology; (2) outline the spectral characteristics of key alteration minerals in sandstone-type uranium deposits within major basins of northern China; (3) comprehensively elaborate on the current application status of this technology in alteration mineral mapping, oxidation–reduction zone delineation, and metallogenic fluid tracing in the sedimentary basins of northern China (including the Qaidam, Ordos, Erlian and Songliao Basins); (4) deeply discuss the challenges currently faced by the technology, and propose future development directions and application recommendations tailored to the characteristics of sandstone-type uranium deposits, with the goal of promoting the further application and development of this technology in the field of sandstone-type uranium exploration.

2. Technical Principles

When incident light interacts with a material, specific wavelengths are absorbed. This absorption behavior is a spectral manifestation of the material's internal structure, trace elements, and indicator ions [36–40]. Generally, after photons interact with atoms and molecules within a mineral crystal, electrons in certain atoms or molecules absorb specific

amounts of light energy. In the visible–near-infrared (VNIR) and shortwave infrared (SWIR) regions (approximately 0.4–2.5 μm), molecular vibrations and electronic transitions are the primary interactions between matter and electromagnetic waves. Electronic transitions occur within the 400–1000 nm wavelength range, producing spectral features. In the 1000–2500 nm range, absorption of energy by atoms and molecules can cause changes in dipole moments, leading to vibrational transitions and resulting characteristic spectral bands. The spectral range utilized by core spectral technology (approximately 0.4–2.5 μm) primarily targets absorption features related to functional groups including C-H (methyl, methylene, methoxy, carboxyl, aryl, etc.), hydroxyl O-H, sulfhydryl S-H, and amino N-H. Their combination and first overtone modes are located in the 1300–2500 nm region [41–43].

Most alteration minerals in sandstone-type uranium deposits contain varying amounts of metal ions (e.g., Fe^{2+}, Fe^{3+}, Mn^{2+}) and anionic groups such as OH^- and CO_3^{2-}, as well as specific structural units. For instance, illite, montmorillonite, and kaolinite contain Al-OH groups; chlorite contains Mg-OH and Fe-OH groups; calcite and dolomite contain CO_3^{2-} groups. These minerals exhibit diagnostic spectral absorption features within the wavelength range (approximately 0.4–2.5 μm) employed by core spectral technology. Spectral absorption characteristics include wavelength position, depth, and width at half maximum (Figure 4A). These parameters are determined by the mass and number of atoms within the functional groups, their geometric arrangement, and the interatomic bonding forces, directly reflecting the mineral composition and crystal structure [44]. For example, the full width at half maximum (FWHM) refers to the width of the spectral feature at half the absorption depth. It is related to the temperature of mineral formation; a smaller FWHM generally corresponds to higher crystallinity, which can be associated with higher formation temperatures or slower crystal growth rates. The wavelength position is the location of the absorption feature, typically defined as the wavelength of minimum reflectance (maximum absorption depth). This position can shift due to elemental substitutions, such as the replacement of Al^{3+} by Fe^{2+} or Mg^{2+} in mica, which causes a shift in the Al-OH absorption feature. The intensity ratio (IC value) is the ratio of the absorption intensities of characteristic mineral peaks, often expressed as the ratio of the depth of a specific alteration mineral feature to the depth of the ubiquitous water absorption feature. This ratio provides information on the mineral's crystallinity. The IC value is influenced by both the temperature and chemical environment during mineralization, as well as clay weathering within the alteration system [33]. For example, in micaceous minerals, the IC value is positively correlated with crystallinity; higher IC values indicate better crystallinity and thus higher formation temperatures. The shape and depth of diagnostic spectral absorption bands are primary criteria for mineral identification and semi-quantitative estimation [12]. Peak intensity refers to the normalized absorption depth of a spectral feature, which is proportional to the relative abundance of the target mineral within the measured area. Theoretically, according to the Beer-Lambert law, this normalized value generally exhibits a positive correlation with mineral content. This relationship has been well-validated and widely applied in previous studies (Figure 4B,C) [45,46]. In the study of metallogenic environments in sandstone-type uranium deposits, these spectral parameters have clear geological implications: shifts in absorption peak wavelength position (Pos) can be used to trace fluid temperature, pH, and sources—for example, a short-wavelength shift of the illite 2200 nm absorption peak (<2205 nm) typically indicates higher-temperature, acidic fluid activity associated with deep hydrothermal or uranium-rich fluid centers; absorption depth (Depth) is positively correlated with the relative abundance of the target mineral, allowing semi-quantitative assessment of alteration intensity and delineation of oxidation–reduction transition zones—for example, in the Yuejin-II sandstone-type uranium deposit in the Qaidam Basin, sharp increases in chlorite or carbonate absorption depth often coincide

spatially with uranium mineralization intervals [8]; FWHM reflects mineral crystallinity, with smaller FWHM values indicating higher crystallization temperatures, which can help distinguish hydrothermal chlorite (smaller FWHM) from diagenetic chlorite (larger FWHM). The comprehensive interpretation of these parameters provides important constraints for reconstructing the physicochemical conditions (pH, Eh, temperature) of ore-forming fluids and the evolution of the metallogenic environment.

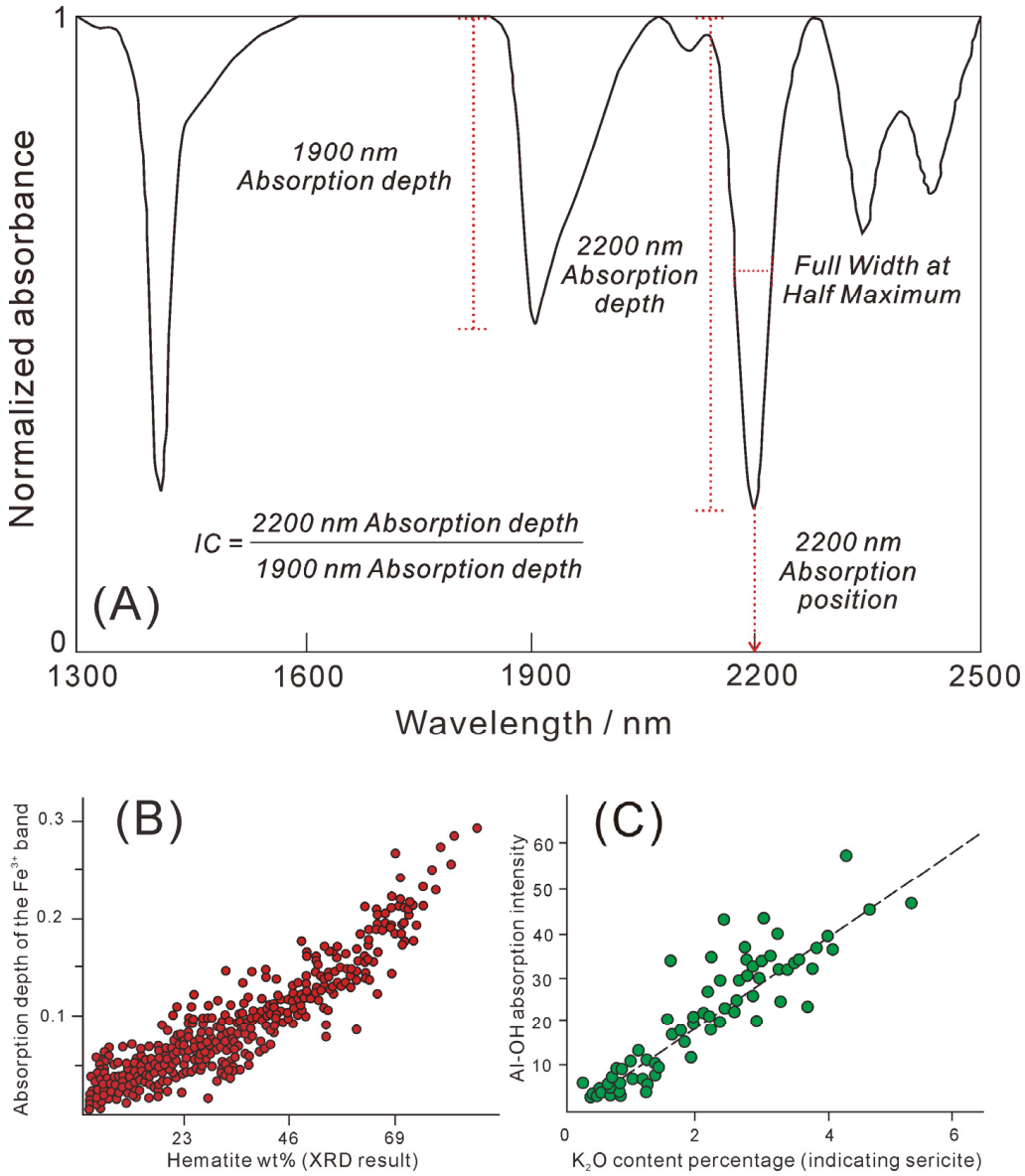

Figure 4. (**A**) Schematic diagram illustrating spectral feature parameters—using the short-wave infrared region as an example. (**B**,**C**) Distribution diagrams showing the correlation between alteration mineral absorption intensity and content: (**B**) demonstrates the positive correlation between hematite content measured by XRD and the absorption depth of the Fe^{3+}-related band; (**C**) shows the positive correlation between K_2O content in sericite and the absorption intensity of the Al-OH feature (after [45,46]).

3. Main Alteration Types and Spectral Characteristics of Sandstone-Type Uranium Deposits

In sandstone-type uranium deposits, low-temperature alteration minerals constitute the main alteration types, generally including clay alteration, carbonatization, and hematitization. The minerals involved primarily comprise kaolinite, montmorillonite, illite, chlorite,

calcite, dolomite, gypsum, hematite, limonite, and pyrite (Figures 2 and 3) [12]. Most alteration minerals, especially those closely associated with mineralization such as chlorite, carbonates, and clay minerals, can be identified using core spectral technology. This paper primarily outlines the spectral characteristics of several common minerals found in sedimentary basin sandstone-type uranium deposits (Figure 5).

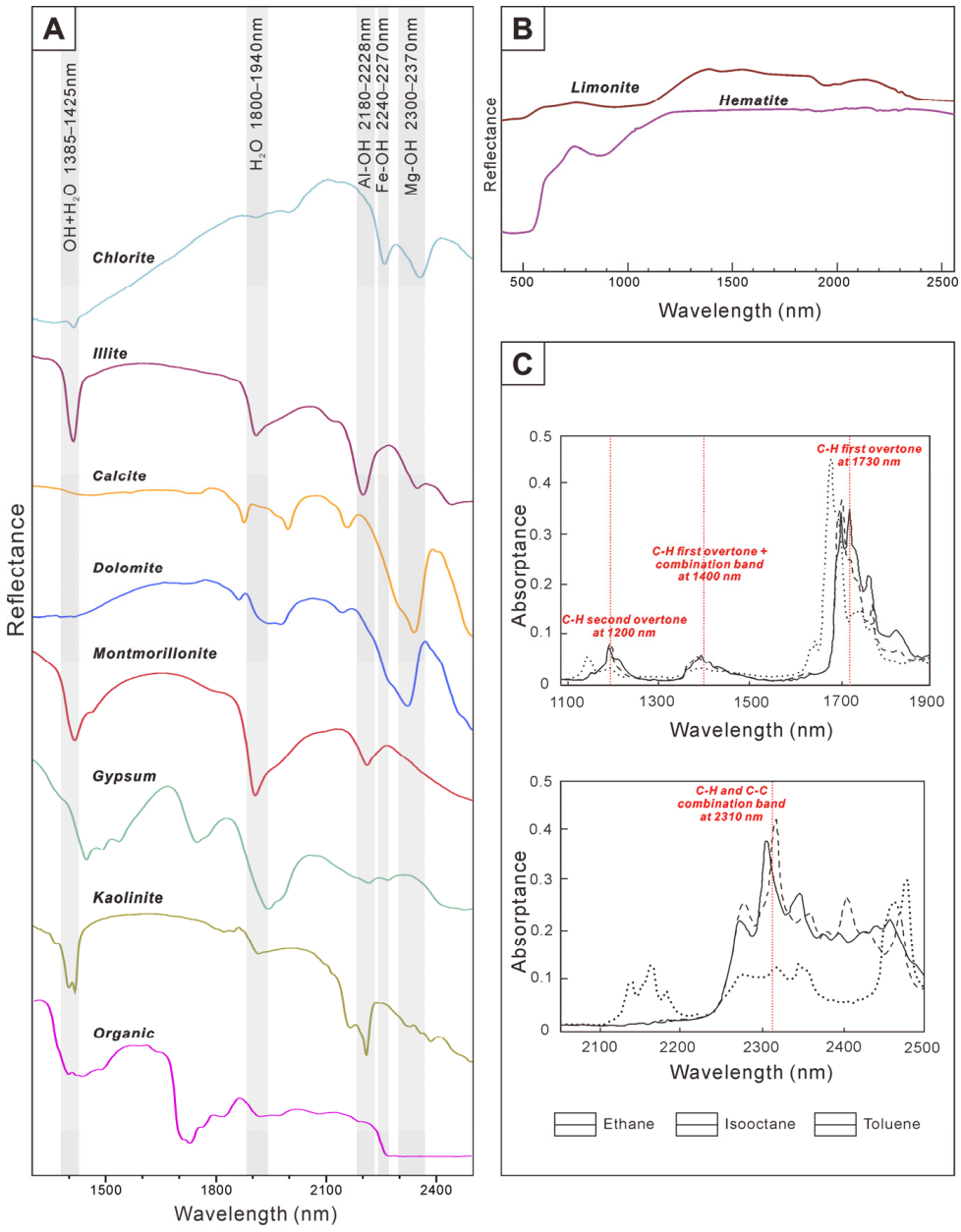

Figure 5. (**A**) Typical short-wave infrared (SWIR) spectral characteristics of clay minerals, chlorite, carbonate minerals, gypsum, and organic matter, modified after [8]. (**B**) Spectral curves of iron oxides, sourced from the USGS spectral library. (**C**) Absorption spectra of hydrocarbons, modified after [47]. The two absorption bands centered at 1730 nm and 2310 nm are commonly used for identifying petroleum in rocks. Note that panel (**C**) displays absorption (**A**) spectra, whereas panels (**A**,**B**) display reflectance (R) spectra. For opaque surfaces (e.g., rocks), absorption A is approximately related to reflectance R by $A \approx 1 - R$.

3.1. Clay Minerals

Clay minerals are the most common and information-rich type of alteration minerals in sandstone-type uranium deposits. They are hydrous silicates with layered structures,

constituting the main mineral components of clay rocks and soils, and are widely distributed in sedimentary rocks. In sandstone-type uranium deposits, the main clay minerals involved are kaolinite, montmorillonite, and illite. All are hydroxyl-bearing minerals and can be identified in the short-wave infrared (SWIR) region (1.3–2.5 μm) (Figure 5A).

3.1.1. Kaolinite

Kaolinite has the chemical formula $Al_4[Si_4O_{10}](OH)_8$, primarily formed by the weathering of feldspars and other silicate minerals or under acidic conditions. Kaolinite is an Al-OH mineral, spectrally characterized by a secondary absorption feature near 2160 nm and a main absorption feature near 2200 nm, forming a diagnostic doublet (Figure 5A) that allows for easy distinction from other clay minerals. Kaolinite has been identified in close spatial association with uranium mineralization in some basins, such as the Qianjiadian deposit (Figure 3F) and the Saihan Formation in the Sangendalai Sag (Figure 3G); however, its abundance can vary and is not always a direct indicator of ore-grade mineralization (see Section 4.1). As a typical indicator mineral for acidic environments, kaolinite predominantly occurs in the oxidized subzone or strongly leached zone of interlayer oxidation zones.

3.1.2. Illite

Illite, also known as hydrous mica, has the ideal chemical composition $K < 1(Al,R^{2+})_2[(Si,Al)Si_3O_{10}][OH]_2 \cdot nH_2O$ and is often formed by the weathering of muscovite and K-feldspar. Illite is also an Al-OH mineral, exhibiting a characteristic Al-OH absorption feature around 2200 nm, a mixed H_2O and OH^- absorption feature near 1400 nm, and an H_2O absorption feature around 1900 nm (Figure 5A). Its spectral characteristics in the SWIR region are similar to those of muscovite and sericite. The wavelength position of the absorption peak near 2200 nm for this mineral group is not fixed and tends to shift to shorter wavelengths with an increasing content of four-fold coordinated aluminum (Al^{IV}) in the mineral lattice. The shift range is approximately 2195–2220 nm, with a maximum amplitude of nearly 30 nm [48]. Short-wavelength illite (<2205 nm) typically indicates formation in higher temperature, relatively acidic fluid environments, possibly associated with magmatic–hydrothermal activity or upwelling of deep-seated fluids, and is often closely related to the activity centers of U-bearing fluids. Long-wavelength illite (>2210 nm) is more commonly formed in lower temperature, neutral to weakly alkaline diagenetic environments. Illite is associated with uranium mineralization in some basins, such as the Qigequan sandstone-type uranium deposit in the Qaidam Basin (Figure 3B) [18].

3.1.3. Montmorillonite

Montmorillonite $(Na,Ca)_{0.33}(Al,Mg)_2\ [Si_4O_{10}](OH)_2 \cdot nH_2O$ is a layered mineral composed of extremely fine-grained hydrous aluminum silicates. It typically forms during early diagenesis or in alkaline environments; however, some montmorillonite can also form under reducing conditions. In the mineralized zones of sandstone-type uranium deposits, its abundance often shows a negative correlation with kaolinite content, as observed in the Qianjiadian sandstone-type uranium deposit in the Songliao Basin [13]. Under specific temperature-pressure conditions, montmorillonite can transform into illite (forming I/S mixed layers). Montmorillonite is also an Al-OH mineral, with its characteristic absorption feature located near 2215 nm, close to the Al-OH absorption of illite (Figure 5A). Current SWIR studies do not heavily emphasize a paragenetic relationship between montmorillonite and uranium mineralization, but it can serve as an indirect indicator for orebody characteristics, such as mineralization intensity. The relationship between montmorillonite and uranium mineralization is mainly reflected in two aspects: First, montmorillonite has a large specific surface area and exchangeable interlayer cations, giving it a strong adsorption capacity for U^{6+}, which can temporarily enrich uranium before the formation of a reducing

environment. Second, the transformation of montmorillonite to illite (I/S mixed layers) is an important potassium-consuming reaction during diagenesis; the cations released and changes in geochemical conditions during this transformation may affect the stability of uranium-bearing fluids. However, in most sandstone-type uranium deposits, montmorillonite is often associated with the diagenetic background rather than directly indicating mineralization events, and thus should not be used alone as a prospecting indicator.

3.2. Chlorite

Chlorite has the general chemical formula $Y_3[Z_4O_{10}](OH)_2 \cdot Y_3(OH)_6$, where Y is primarily Mg^{2+}, Fe^{2+}, Al^{3+}, and Fe^{3+}, making it a Mg-, Fe-bearing silicate mineral. Its spectral absorption characteristics result from the combined effects of Mg-OH and Fe-OH, manifested as a main absorption peak between 2330–2350 nm and a secondary absorption peak around 2250–2260 nm (Figure 5A). The Mg-OH absorption peak of chlorite near 2340 nm is close to the asymmetric single peak characteristic of carbonates in the 2300–2400 nm range. Therefore, the identification of chlorite in sandstone-type uranium deposits primarily relies on the Fe-OH absorption peak around 2250 nm because the Mg-OH peak of chlorite overlaps significantly with carbonate absorption, whereas the Fe-OH peak near 2250 nm is unique to chlorite and not shared by most carbonate minerals [8]. Chlorite associated with uranium mineralization is present in most basins. For example, significant amounts of chlorite intimately intergrown with uranium minerals have been found in the Qigequan and Yuejin-II sandstone-type uranium deposits in the Qaidam Basin (Figure 3A,D,E) [8], as well as in the Jingchuan sandstone-type uranium deposit in the Ordos Basin (Figure 3H) [7]. The presence of chlorite is often linked to reducing environments or hydrothermal activity. Studies on chlorite alteration in the Nalinggou uranium deposit suggest its formation is closely related to oxidation–reduction reactions, the involvement of organic matter/hydrocarbon fluids, and diagenetic–hydrothermal fluid activity [49].

3.3. Carbonate Minerals

Common carbonate minerals in sandstone-type uranium deposits mainly include calcite ($CaCO_3$), dolomite ($CaMg(CO_3)_2$), and siderite ($FeCO_3$) [12]. All exhibit characteristic absorptions in the SWIR region, but their positions and shapes differ slightly. The main absorption peaks for calcite and dolomite, caused by vibrations of the CO_3^{2-} group, are located near 2320–2350 nm. Calcite's characteristic peak is near 2340 nm, largely overlapping with the Mg-OH absorption of chlorite, while dolomite's absorption position is slightly shorter than that of calcite (Figure 5A). Carbonate minerals, like chlorite, are alteration minerals closely associated with uranium mineralization. Carbonates intimately intergrown with uranium minerals are widespread in most basins, such as the Qaidam and Ordos Basins (Figure 3C–E,H) [7,8,18]. The co-occurrence of carbonate and chlorite is common in basins of northern China (Figure 3H) [7,8,16]. It has been suggested that zones where carbonate and chlorite coexist may represent interfaces where geochemical parameters like pH change, potentially facilitating the decomposition and precipitation of uranium minerals [16]. Identifying the type and distribution of carbonate minerals aids in understanding the properties of ore-forming fluids and water-rock interaction processes. For instance, the carbonate minerals in the Yuejin-II sandstone-type uranium deposit in the Qaidam Basin are predominantly calcite [8]. This calcite-dominated carbonatization reflects a neutral to alkaline fluid environment, with the altering fluid being rich in Ca^{2+} and containing a certain concentration of carbonate species [7].

3.4. Gypsum

Gypsum exhibits a characteristic absorption peak at 1750 nm (Figure 5A), a unique spectral feature enabling its unambiguous identification. In some basins, gypsum can also

serve as a mineralization indicator. For example, SWIR analysis of the Pengyang sandstone-type uranium deposit in the Ordos Basin revealed that the most prominent feature of mineralized intervals is a sharp increase in gypsum content [14]. The relationship between gypsum and uranium mineralization varies among different basins. In the Pengyang deposit, the sharp increase in gypsum content may reflect the precipitation of sulfate minerals resulting from the injection of reducing, acidic fluids during mineralization [14]. The mechanism can be explained as follows: acidic hydrocarbon-bearing fluids (rich in H_2S) mix with supergene oxygen–uranium-bearing fluids, oxidizing H_2S to SO_4^{2-}, which then combines with Ca^{2+} in the formation to precipitate gypsum; simultaneously, U^{6+} is reduced to U^{4+} and precipitates as ore. Thus, gypsum can serve as a mineralization indicator in this deposit, but its applicability needs to be verified based on the specific fluid characteristics of each basin.

3.5. Iron Oxides

Hematite (Fe_2O_3) and limonite ($2Fe_2O_3 \cdot 3H_2O$) are indicative minerals of oxidizing environments, commonly found in sedimentary strata. Limonite, in particular, is extensively developed in shallow, near-surface parts of some basins, such as the shallow portion of the Yuejin-II sandstone-type uranium deposit in the Qaidam Basin (Figure 2) [8]. Limonite is also developed in the Jingchuan uranium deposit in the Ordos Basin, where it decreases in abundance and transitions to pyrite within the mineralized zone (Figure 3I) [7]. These iron oxides exhibit broad absorption features in the visible-to-near-infrared (VNIR) region (especially 400–1200 nm) due to electronic transitions of Fe^{3+}. Hematite typically shows absorptions around ~550 nm and ~850 nm, while limonite's main absorption peak is located around ~950 nm (Figure 5B) [47]. The ability to differentiate hematite from limonite (hydrated iron oxide) allows for more refined interpretation of oxidation intensity and water-rock interaction history, as hematite typically indicates more oxidizing and/or higher-temperature conditions. Utilizing VNIR data allows for effective identification and differentiation of these iron oxides, enabling detailed delineation of the oxidation front position within interlayer oxidation zones.

3.6. Organic Matter and Hydrocarbons

Reducing agents such as organic matter or oil and gas are often present in the reduction zone. Many sandstone-type uranium deposits in the basins of northern China are characterized by the co-exploitation of oil and uranium. Such deposits commonly have spatial and genetic associations with hydrocarbons. For example, the Qaidam Basin hosts extensive oilfields, and significant amounts of oil and gas are developed in the Neogene Shizigou Formation at depth in both the Qigequan and Yuejin-II sandstone-type uranium deposits within the basin (Figure 2), showing a close relationship with uranium mineralization, as discussed in the Qaidam Basin case study (Section 4.2). In basins where oil-gas and uranium coexist, using core hyperspectral technology to directly identify hydrocarbon anomalies is of great significance for evaluating reducing capacity and delineating reduction alteration zones. Hydrocarbons exhibit characteristic absorptions due to C-H bond vibrations. The combination and overtone modes of C-H covalent bond vibrations produce distinct absorption features in the 1000–2500 nm wavelength range [50,51], allowing hyperspectral technology to be directly applied for hydrocarbon analysis and identification. Wavelengths around 1730 nm, 1755 nm, and 2310 nm are three characteristic SWIR absorption features for hydrocarbons [50,52]. Considering the potential coexistence of clay minerals and carbonates in drill core samples from sandstone-type uranium deposits, the observable hydrocarbon absorptions are likely to be primarily at 1730 nm and 1755 nm

(Figure 5C). The absorption band near 1730 nm is particularly important (Figure 5A), as there is minimal mineral interference at this wavelength [47].

4. Application Practices of Core Spectral Technology in Sandstone-Type Uranium Deposits Within Basins of Northern China

In recent years, core spectral technology has been successfully applied in major uranium-bearing basins of northern China, including the Ordos, Songliao, Erlian, and Qaidam Basins, achieving remarkable results [8,12–17]. Research indicates that the dominant alteration types vary among different basins (Figure 2) [7,8,13,18,19]. The widespread occurrence of alteration across basins in northern China, coupled with the diversity of alteration assemblages in different basins, provides the foundation for the practical application of this technology. Borehole alteration mineral mapping represents the most fundamental and core application of core hyperspectral technology. Its primary objective is to transform continuous spectral data from drill cores into geologically meaningful, vertical profiles showing variations in mineral species and relative abundances, thereby constructing a "log of alteration minerals" for individual boreholes. Compared to traditional descriptions based on sparse sampling and visual inspection, such continuous mineralogical logs can reveal the vertical zoning patterns of alteration minerals within the ore-bearing horizon and their intrinsic relationships with lithology and uranium mineralization in a more detailed and objective manner. In recent years, Chinese scholars have conducted systematic borehole alteration mineral mapping in sandstone-type uranium deposits across multiple basins using independently developed CMS series core spectral scanners (e.g., CMS350A/B) and portable field spectrometers (e.g., ASD LabSpec4), yielding significant insights.

4.1. Songliao Basin: Qianjiadian Uranium Deposit

The Songliao Basin is the largest Meso-Cenozoic continental sedimentary basin in northeastern China. The Qianjiadian Depression in its southwestern part is a significant enrichment area for sandstone-type uranium deposits (Figure 6A,B). The Upper Cretaceous Yaojia Formation (K_2y) serves as the main ore-bearing horizon. The lithology primarily consists of light gray, gray, light red, and variegated fine-grained sandstones, intercalated with red and gray mudstones, carbonaceous mudstones, and silty mudstones. It exhibits a typical positive rhythmic sequence, characteristic of a braided river depositional system. Multiple stable mudstone aquicludes form a favorable "mudstone-sandstone–mudstone" structure, providing good pathways for fluid migration and storage space for alteration minerals.

4.1.1. Borehole Alteration Mineral Mapping

Li et al. (2020) [13] employed the CMS350A fully automated digital core spectral scanner (developed by the Nanjing Geological Survey Center, China Geological Survey) to conduct high-resolution (5 cm sampling interval) continuous spectral scanning on cores from 85 boreholes. Through interpretation using TSG software, they constructed vertical distribution maps of clay minerals for boreholes within the mining area and its periphery (Figure 7). These maps clearly reveal the vertical evolution of clay minerals within the Yaojia Formation: in barren boreholes (Figure 7B), the clay mineral assemblage is relatively simple, dominated by montmorillonite or I/S mixed-layer clays. In contrast, in mineralized boreholes, kaolinite content increases significantly, exhibiting a clear "antithetic" relationship with montmorillonite (Figure 7A). More importantly, kaolinite enrichment is not uniformly distributed but concentrated in specific intervals, showing good spatial correspondence with uranium mineralization zones (e.g., borehole QIV-88-112 in Figure 6D). This discovery provides crucial mineralogical evidence for subsequent fluid tracing and metallogenic mechanism studies. While kaolinite generally correlates with mineralization

in this area, this relationship is not absolute; a multi-parameter approach integrating kaolinite, montmorillonite, illite, and iron oxide content is recommended for optimal analysis.

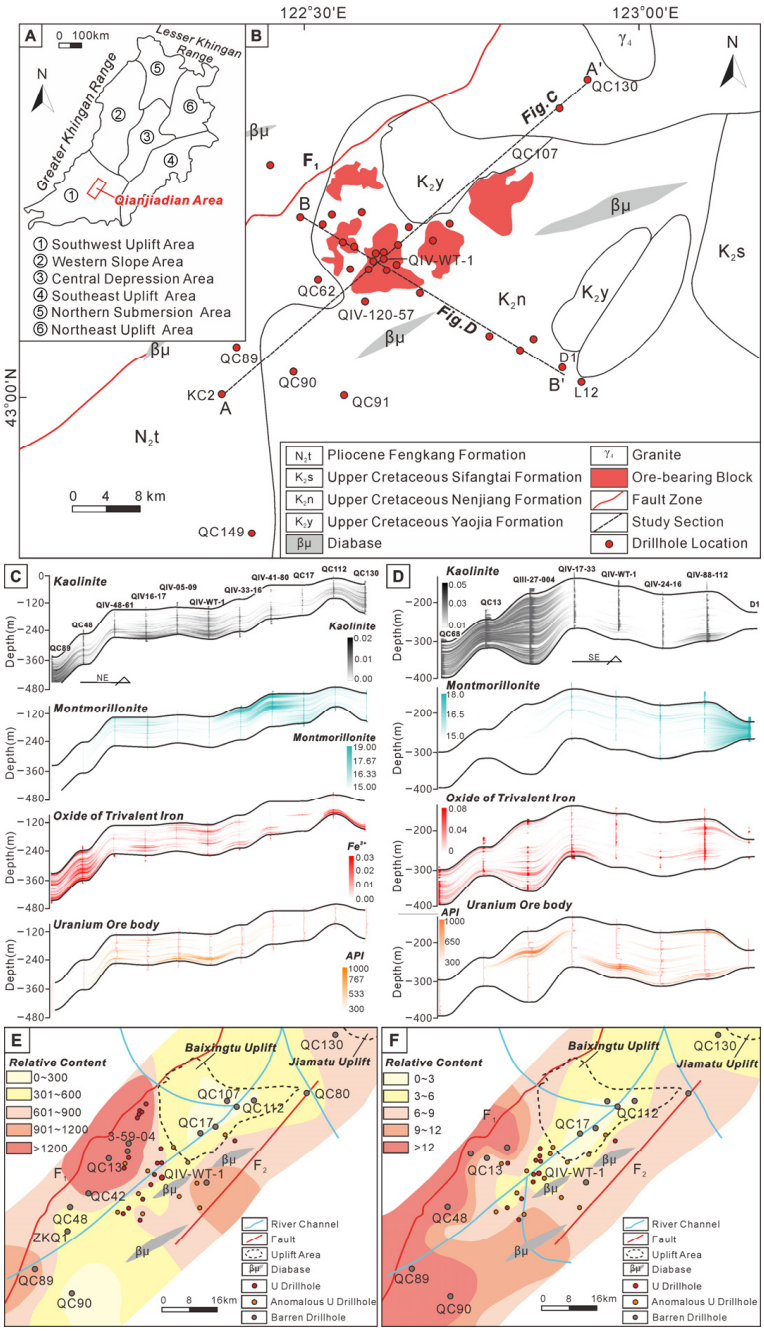

Figure 6. (**A**,**B**) Regional geological sketch map of the Qianjiadian sandstone-type uranium deposit in the southwestern Songliao Basin, showing the location of the study area and boreholes (modified after [13]). (**C**) WS-NE trending cross-section A-A′ illustrating the distribution of alteration minerals in the lower member of the Upper Cretaceous Yaojia Formation. Key observation: From the oxidation zone (red sandstones, high kaolinite + Fe^{3+} oxides) to the reduction zone (gray sandstones, high montmorillonite + illite + pyrite), a distinct transition zone characterized by moderate kaolinite + montmorillonite (I/S) and high pyrite + ankerite is developed, and the uranium orebodies are hosted in this transition zone. (**D**) NW-SE trending cross-section B-B′ showing a symmetrical zoning pattern (red → gray → red sandstone). Note: The kaolinite content in the red sandstone at the SE end is significantly lower than that at the NW end, interpreted by the Li et al. (2020) [13] as being related to the proximity to the deep-seated F_1 fault and the influence of deep-seated acidic, hydrocarbon-bearing fluids. (**E**) Planar distribution map of relative kaolinite content in the lower member

of the Yaojia Formation. The high-value area extends from the NE-trending deep-seated fault towards the mining area. (**F**) Planar distribution map of relative ferric iron oxide content in the lower member of the Yaojia Formation. The high-value area exhibits a "U-shaped" distribution surrounding the mining area and uplifted zones, with high contents located to the WS and WN of the mining area. Interpretation: The spatial gradient in mineral content indicates that acidic, hydrocarbon-bearing fluids were primarily de-rived from the NE direction, whereas oxygenated, uranium-bearing fluids originated mainly from the WS and WN directions. The orebodies are precisely situated at the confluence of these two fluids, within the gradient zone of kaolinite variation and the transition zone of ferric iron oxides. This figure demonstrates how SWIR-based alteration mapping can be used for large-scale fluid system reconstruction and orebody targeting.

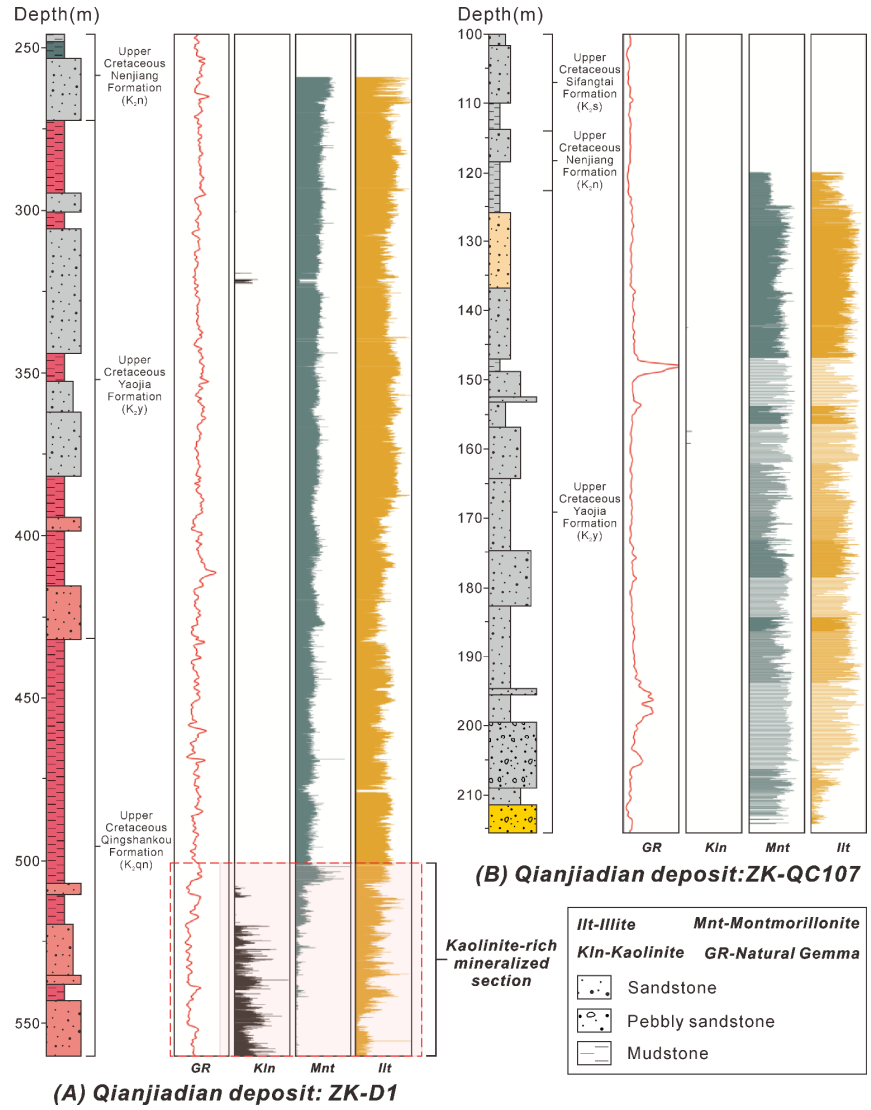

Figure 7. Vertical distribution of clay minerals in representative boreholes from the periphery of the Qianjiadian deposit, southwestern Songliao Basin (modified after [13]). (**A**) Mineralized borehole D1 (located at the orebody margin). Key observation: Within the kaolinite-rich interval (highlighted by the yellow band), a distinct "antithetic" relationship is observed between kaolinite and montmorillonite—kaolinite abundance increases sharply while montmorillonite decreases. Uranium mineralization (shown by the gamma-ray log, GR curve) coincides with the kaolinite peak and the montmorillonite trough, indicating that the orebody is located within the gradient zone of clay mineral transformation. This relationship reflects alternating acidic (kaolinite-precipitating) and alkaline (montmorillonite-stabilizing) fluid conditions. (**B**) Barren borehole QC107. The clay mineral assemblage is relatively simple, dominated by montmorillonite or I/S mixed-layer clays. No significant kaolinite enrichment or anti-thetic relationship is observed, and the gamma-ray anomaly

is weak. Significance: The antithetic relationship between kaolinite and montmorillonite can serve as a proximal indicator of the oxidation–reduction transition zone and can be used to locate potential orebodies. However, kaolinite enrichment alone is not an absolute indicator; integrated assessment combining kaolinite, montmorillonite, illite, and iron oxide data is recommended to improve prospecting reliability.

4.1.2. Delineation of Oxidation-Reduction Zones

Accurate delineation of oxidation-reduction zoning is one of the core objectives in studying metallogenic regularities and conducting prospecting predictions for sandstone-type uranium deposits. Traditional methods for defining oxidation-reduction zones primarily rely on visual observation of rock colors (red, yellow, gray, green) and analysis of a limited number of geochemical samples. This approach is not only highly subjective but also struggles to achieve continuous and quantitative characterization. Its limitations become particularly pronounced in complex mineralized zones characterized by gradual color transitions and multi-stage fluid overprinting. Previous studies have demonstrated that oxidation-reduction environments can be inferred using alteration minerals and their assemblages [53]. The presence of ferric iron oxides and hydroxides (e.g., hematite, limonite) typically indicates oxidizing conditions. Conversely, ferrous iron sulfides (e.g., pyrite, marcasite), which can only form or be preserved under reducing conditions, serve as indicators of reducing environments [16]. Among these, iron oxides such as hematite and limonite exhibit broad absorption features in the visible to near-infrared (VNIR) region (particularly 400–1200 nm) due to electronic transitions of Fe^{3+} making them readily identifiable by core spectral technology. Therefore, by leveraging this technology to identify the types, abundances, and assemblages of characteristic minerals within different zones, a refined and quantitative characterization of oxidation-reduction zoning can be achieved.

Based on the spectral mapping results from 85 boreholes, Li et al. (2020) [13] also constructed alteration mineral distribution maps for the lower member of the Yaojia Formation along the WS-NE A-A′ cross-section and the NW-SE B-B′ cross-section (Figure 6C,D). These cross-sections clearly reveal the mineralogical evolution sequence from the oxidation zone to the reduction zone. Along A-A′, from WS to NE, rock color gradually transitions from red to gray sandstones, corresponding to systematic changes in alteration assemblages: the oxidation zone is characterized by high abundance of "kaolinite + Fe^{3+} oxides" (hematite, goethite), indicating a strongly oxidizing environment; progressing northeastward into the oxidation–reduction transition zone, the assemblage shifts to moderate abundances of "kaolinite + montmorillonite (I/S mixed layers)", accompanied by high abundances of "pyrite + ankerite". The appearance of this assemblage marks the transition from oxidizing to reducing conditions and represents the most favorable site for uranium mineralization. Further into the reduction zone, the assemblage is dominated by high abundances of "montmorillonite (I/S) + illite + pyrite", indicating a stable reducing environment. Along B-B′, a symmetrical zoning pattern of "red sandstone → gray sandstone → red sandstone" is observed, wherein kaolinite content in the red sandstones at the SE end is significantly lower than at the NW end, attributed by the Li et al. (2020) [13] to proximity to the deep-seated F_1 fault and influence of deep-seated acidic, hydrocarbon-bearing fluids.

4.1.3. Tracing of Ore-Forming Fluids

The spatial distribution patterns of alteration minerals provide critical information for interpreting the properties, sources, and migration pathways of ore-forming fluids. Core spectral technology, by identifying spectral parameters of specific minerals, offers key evidence for fluid tracing and delineation of mineralization centers. Li et al. (2020) [13] conducted fluid migration analysis based on mineral content gradients. They constructed planar distribution maps of kaolinite and ferric iron oxides in the lower member of the

Yaojia Formation (Figure 6E,F). The results revealed that the high-value area for kaolinite extends from the NE-trending deep-seated fault towards the mining area, while the high-value area for Fe^{3+} oxides exhibits a "U-shaped" distribution surrounding the mining area and uplifted zones, with high content areas located to the WS and WN. This spatial gradient clearly indicates that acidic, hydrocarbon-bearing fluids were primarily derived from the NE direction at depth, whereas oxygenated, uranium-bearing fluids originated mainly from the WS and WN directions. The ore bodies are precisely situated at the confluence of these two fluids, within the gradient zone of kaolinite content variation and the transition zone of Fe^{3+} oxide distribution. This study represents an exemplary application of hyperspectral data for large-scale reconstruction of fluid systems.

4.2. Qaidam Basin: Yuejin-II Uranium Deposit

The Qaidam Basin is a significant Meso-Cenozoic intracontinental sedimentary basin in northwestern China. In recent years, sandstone-type uranium mineralization closely associated with hydrocarbon fluids has been discovered in the Yuejin-II area of its western part during petroleum exploration (Figure 8A,B). The Cenozoic stratigraphy is fully developed, with the main ore-bearing horizons being the Quaternary Qigequan Formation and the Neogene Shizigou Formation (Figure 8C). The Qigequan Formation primarily consists of pebbly sandstones and sandy conglomerates, intercalated with yellowish-brown argillaceous siltstones and grayish-white marlstones, with locally intense carbonatization. The Shizigou Formation is dominated by grayish-white sandstones and sandy conglomerates, locally interbedded with mudstones; brown oil-impregnated sandstones are commonly observed at its basal contact with the underlying Upper Youshashan Formation. A regional angular unconformity separates these two ore-bearing sequences (Figure 8C).

4.2.1. Borehole Alteration Mineral Mapping

Wu et al. (2026) [8] conducted detailed spectral measurements on cores from three boreholes in the Yuejin-II deposit using an ASD LabSpec4 Hi-Res portable SWIR spectrometer (Malvern Panalytical, Great Malvern, UK). Integrating petrographic observations and XRD validation, they constructed comprehensive alteration mineral logs for the three boreholes (Figure 9) and a mineralization-alteration model diagram (Figure 10). The log from representative borehole ZKII-4 (Figure 9) displays the vertical zoning of alteration minerals from the shallow Qigequan Formation to the deeper Shizigou Formation. The study revealed that uranium mineralization intervals, primarily concentrated near the unconformity, do not correlate with a synchronous enrichment of all alteration minerals but exhibit a strong positive correlation with a sharp increase in the "chlorite + carbonate" assemblage (Figure 9). The absorption intensity curves for chlorite and carbonate fluctuate almost synchronously with the gamma-ray uranium signal within mineralized intervals, forming a distinct peak-to-peak correspondence. In non-mineralized intervals, the abundance variations of these two minerals are relatively subdued or show a negative correlation. This detailed mapping result not only identified the alteration assemblage most closely related to mineralization but also provided a direct basis for tracing stratabound orebodies along the unconformity surface. Notably, Wu et al. (2026) [8] also noted that in intervals with complex lithology (e.g., upper part of Figure 9), the presence of numerous interfering factors makes SWIR interpretation challenging, resulting in noisy data; in contrast, in intervals with relatively homogeneous lithology (e.g., lower part of Figure 9), the SWIR results for mineralization-related alterations correspond well with mineralization position and intensity. This observation supports the challenges discussed later in Section 5.

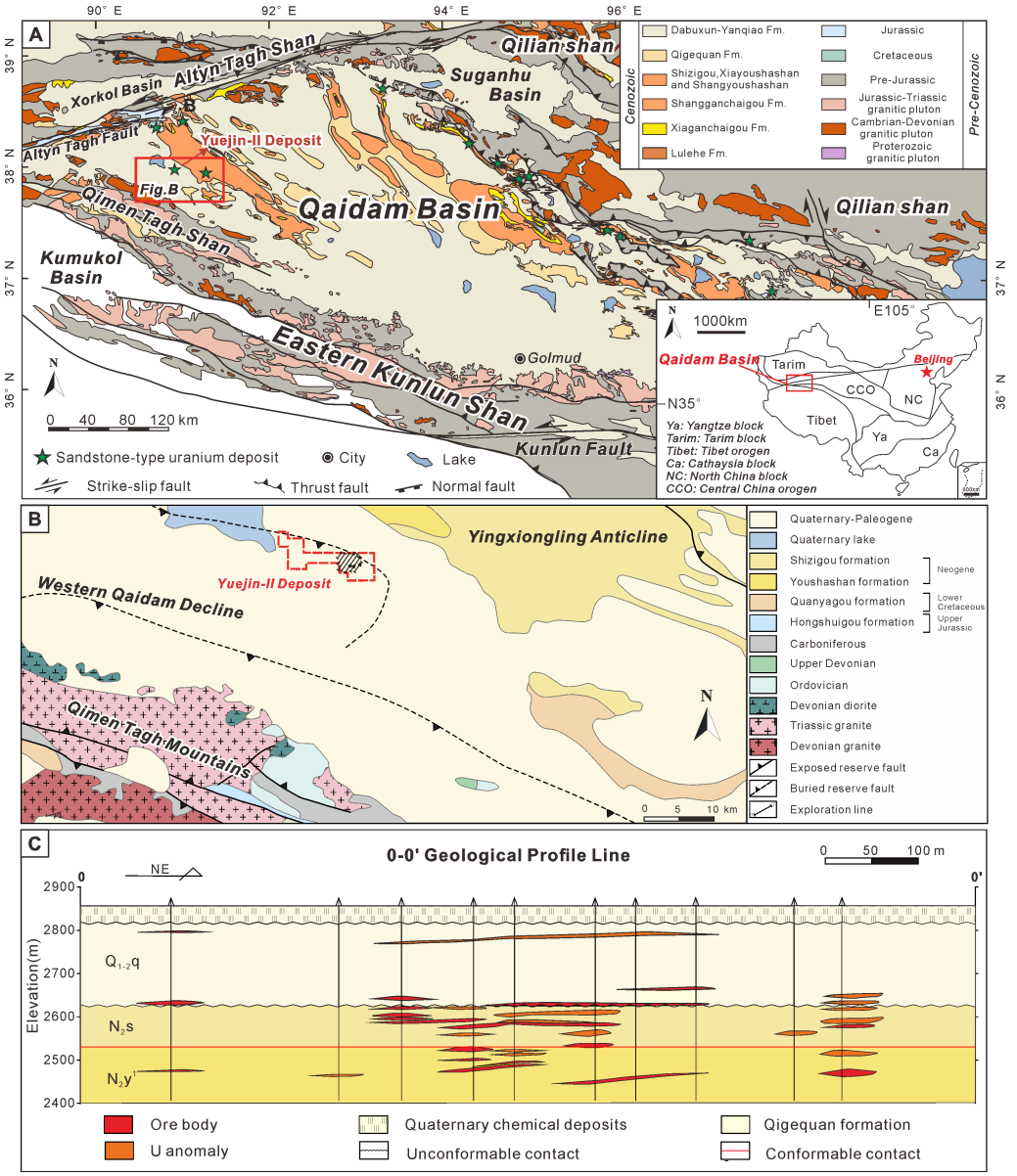

Figure 8. (**A**) Geological map of the Qaidam Basin and the surrounding regions, modified from [54]. (**B**) Geological map of the Yuejin-II mining area in the western margin of the Qaidam Basin, modified after [8]. (**C**) Geological cross-section along exploration line 0-0′, modified after [8], showing that mineralization is primarily hosted in the Quaternary Qigequan Formation and the Neogene Shizigou Formation.

4.2.2. Tracing of Ore-Forming Fluids

Based on the distribution of the chlorite-carbonate assemblage and mineralization in the Yuejin-II mining area, Wu et al. (2026) [8] preliminarily delineated a layered alteration zone extending laterally for over 500 m along the unconformity, which closely coincides spatially with the ore bodies (Figure 10). This discovery confirms the effectiveness of SWIR in identifying key alteration indicators and provides an economical, efficient technical approach for rapidly delineating prospecting targets in similar basins.

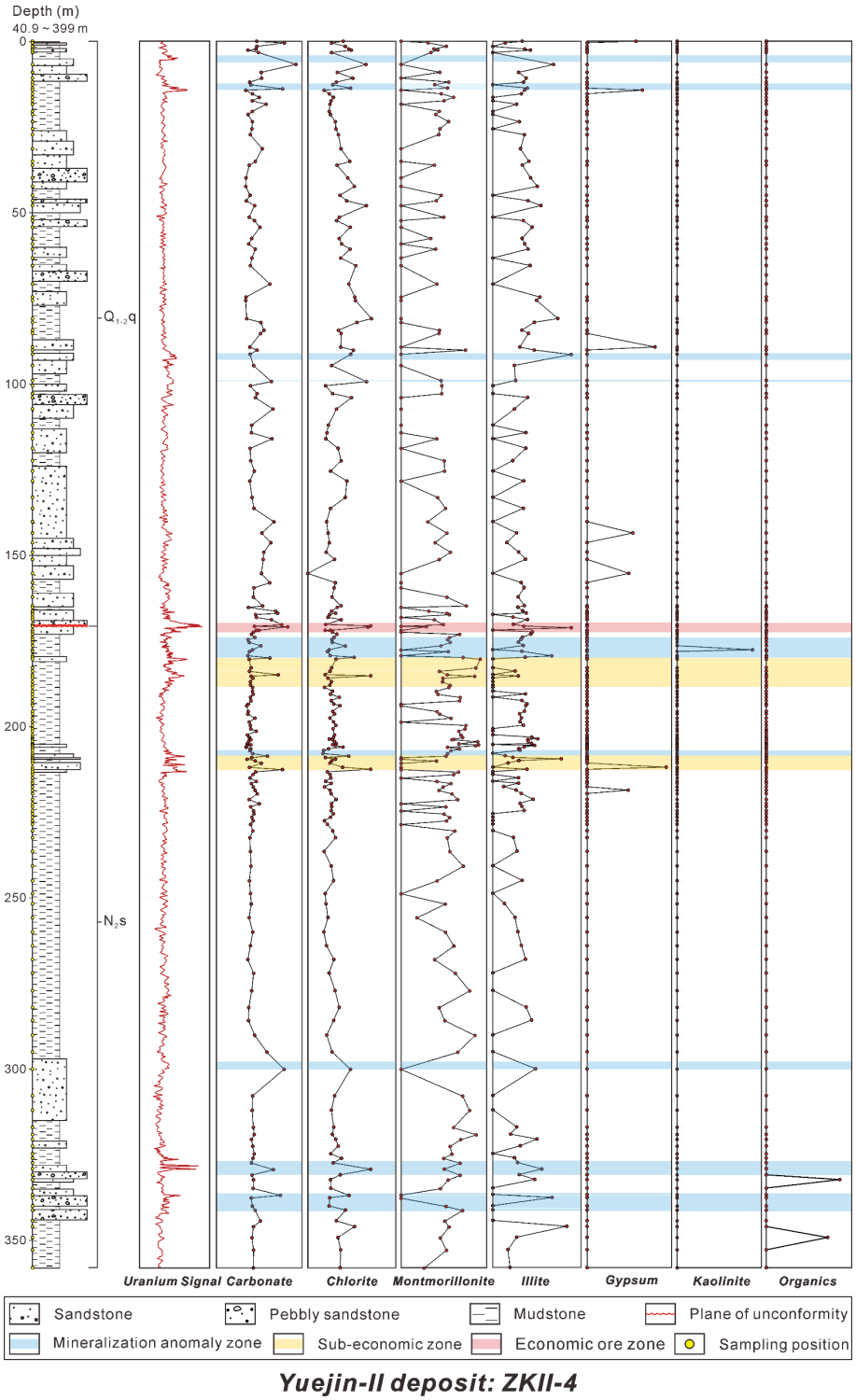

Figure 9. Vertical distribution of alteration minerals in borehole ZKII-4 from the Yuejin-II sandstone-type uranium deposit, western Qaidam Basin, modified after [8]. Spectral data were acquired using an ASD LabSpec4 Hi-Res portable short-wave infrared spectrometer manufactured by Malvern Panalytical, UK. The figure shows that within this borehole, the abundances of carbonate and chlorite exhibit a positive correlation in the uranium mineralization intervals, both showing increases that broadly coincide with variations in the uranium signal. In the upper part, where lithology is complex with numerous interfering factors, SWIR identification is challenging, resulting in relatively noisy data. In the lower part, where lithology is relatively homogeneous with fewer interfering factors, the SWIR results for mineralization-related alterations correspond well with the mineralization position and intensity.

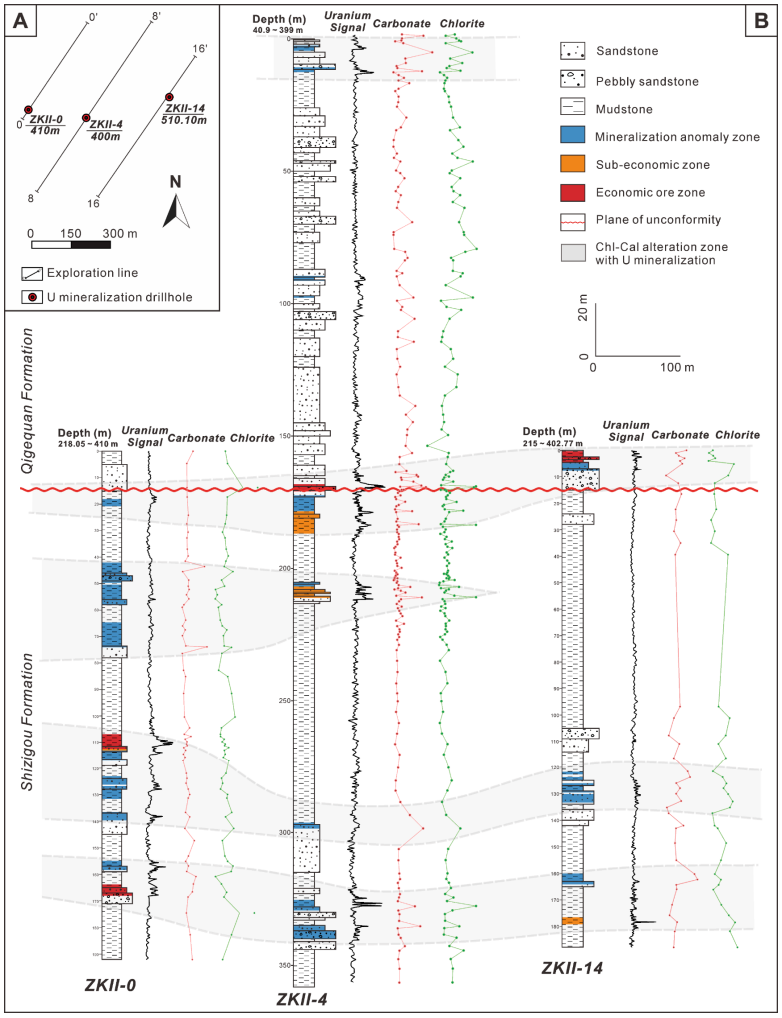

Figure 10. Mineralization-alteration model map of the Yuejin-II mining area, western Qaidam Basin, modified after [8]. (**A**) shows the spatial relationship of the three boreholes in plan view. (**B**) shows that in zones with better mineralization, the correlation between chlorite and carbonate abundances and the uranium signal is stronger, indicating that sharp increases in chlorite and carbonate can, to a certain extent, indicate sandstone-type uranium mineralization.

4.3. Ordos Basin: Pengyang Uranium Deposit

The Ordos Basin, located in north-central China, is the second largest sedimentary basin in the country, covering an area of 250,000 km^2. It hosts one of the most significant sandstone-type uranium mineralization belts in China. In recent years, a deep-seated sandstone-type uranium deposit has been newly discovered in the Pengyang area on its southwestern margin (Figure 11), characterized by large-scale sand bodies, extensive uranium mineralization, and significant thickness. The Lower Cretaceous Luohe Formation serves as the primary ore-bearing horizon. It comprises a set of thick red sand bodies developed under an aeolian depositional system, with lithology predominantly reddish-brown, light yellow, and gray medium- to fine-grained sandstones, locally intercalated with pebbly coarse sandstones, sandy conglomerates, or thin silty mudstones. The top and bottom are bounded by lacustrine mudstones and siltstones, forming a giant "mudstone-sandstone–mudstone" assemblage. The ore bodies are mainly located in the light gray medium- to fine-grained sandstones in the lower part of the Luohe Formation, reflecting the transition from an oxidizing to a reducing environment, which is a key control in uranium mineralization.

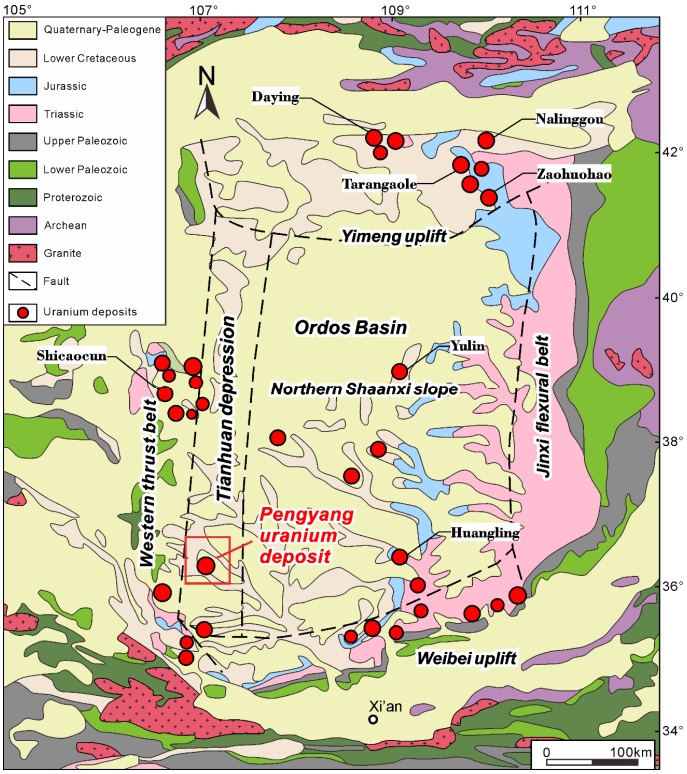

Figure 11. Simplified geological map of the Ordos Basin (modified after [55]), showing the distribution of major sandstone-type uranium deposits and main tectonic boundaries: Yimeng Uplift, Weibei Uplift, Western Margin Thrust Belt, and Jinxi Fold Belt.

4.3.1. Borehole Alteration Mineral Mapping

Zhang et al. (2022) [14] conducted near-infrared spectral scanning on core from borehole ZK1 using a CMS350B core spectral scanner (developed by the Nanjing Geological Survey Center, China Geological Survey), generating a mineral distribution map for the Luohe Formation (Figure 12). The map details the vertical variation of minerals such as illite (including I/S), kaolinite, chlorite, carbonate, gypsum, and iron oxides over a depth interval of ~1050–1450 m. The mineral assemblage within the uranium mineralized interval is distinctly characterized by "illite (I/S) + gypsum + carbonate", with kaolinite observed locally (Figure 12). Compared to non-mineralized wall rocks, the most significant changes are a sharp increase in gypsum content and the near-complete disappearance of iron oxides. This detailed mineral assemblage mapping provides critical constraints for interpreting the nature of the ore-forming fluids (reducing, acidic fluids) and the metallogenic environment (transition from oxidizing to reducing conditions). It is worth noting that carbonatization here has been influenced by late-stage overprinting and contamination from the surrounding rock matrix. Therefore, although its relationship with mineralization is very close [7], the actual abundance of syn-mineralization siderite is not that significant, making it less prominent in spectral testing. Consequently, refining key indicators is essential for effective prospecting.

4.3.2. Tracing of Ore-Forming Fluids

Using near-infrared core spectral scanning technology, Zhang et al. (2022) [14] identified the characteristic mineral assemblage within the uranium mineralized interval of the Luohe Formation as "illite (I/S mixed-layer clays) + gypsum + carbonate", with kaolinite observed locally (Figure 12). Based on this, Zhang et al. (2022) [14] interpreted that the ore-bearing interval was primarily in an alkaline environment during deposition, whereas

reducing, acidic fluids were introduced during mineralization. This provides critical mineralogical evidence for understanding the genesis of this deep-seated deposit.

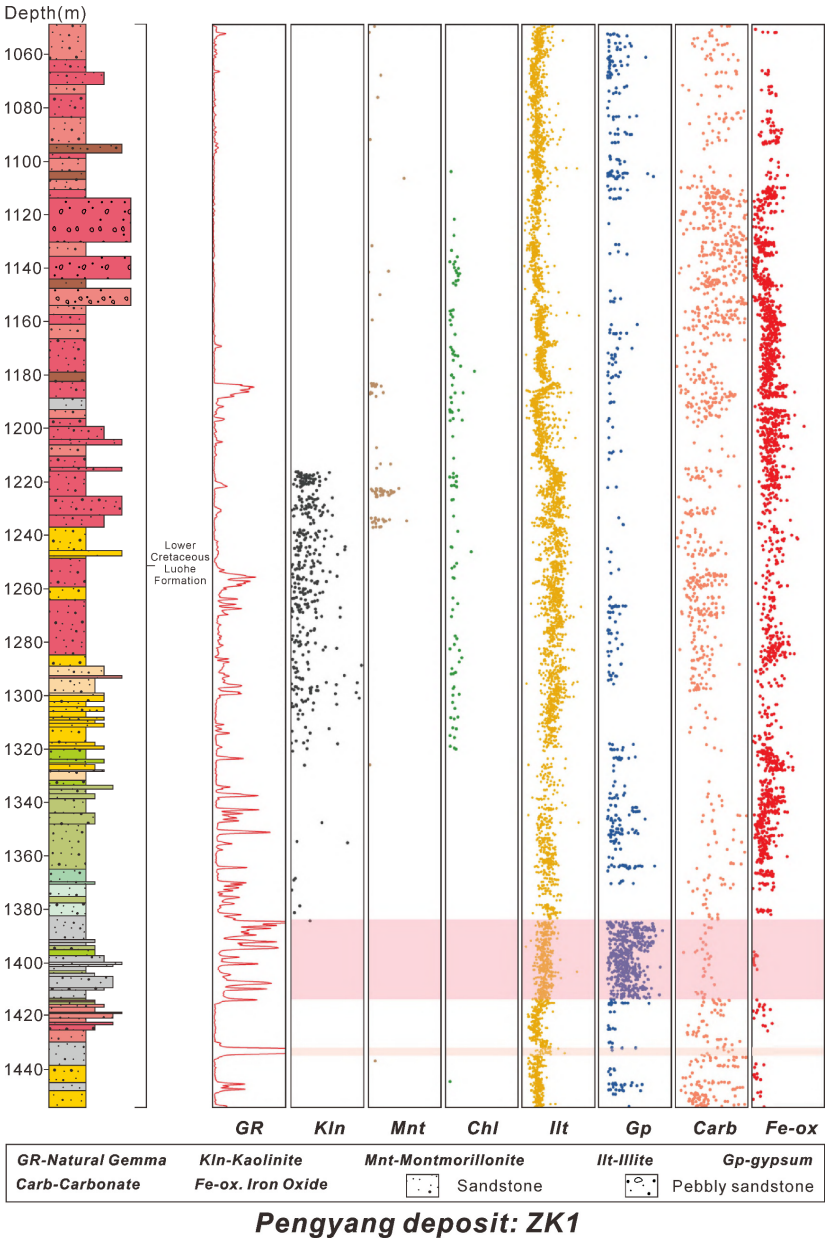

Figure 12. Vertical distribution of alteration minerals in borehole ZK1 from the Pengyang area sandstone-type uranium deposit, southwestern margin of the Ordos Basin, modified after [14]. Spectral data were acquired using a digital core spectral scanner (CMS350B model) developed by the Nanjing Geological Survey Center, China Geological Survey. The figure shows that the mineral assemblage within the uranium mineralized interval of the Lower Cretaceous Luohe Formation in this area is characterized by "illite (including I/S mixed-layer clays) + gypsum + carbonate", with kaolinite observed locally. Compared to the non-mineralized wall rocks above and below, the most significant changes within the mineralized interval are a sharp increase in gypsum content and the near-complete disappearance of iron oxide minerals. The color of the core column in the figure represents the color of the rock.

4.4. Erlian Basin: Sangendalai Sag

The Erlian Basin is an important Meso-Cenozoic sedimentary basin in northern China, hosting abundant oil, gas, coal, and uranium resources. Sandstone-type uranium deposits are predominantly distributed in the Manite and Ulanqab Depressions in the western part

of the basin (Figure 13A). The primary ore-bearing horizon is the upper member of the Saihan Formation, followed by the Erlian and Tenggeer Formations. The uranium source is mainly derived from uranium-rich felsic igneous rocks in the provenance area [9,19,56–63]. In contrast to these depressions, the Chuanjing Depression in the western part previously received limited uranium exploration, resulting in only localized uranium mineralization and anomalies [64]. Recently, through further drilling, a relatively continuous industrial uranium orebody (BYH deposit) was discovered in the slope zone of the southwestern corner of the Sangendalai Sag, northeastern Chuanjing Depression (Figure 13B,C). In this area, the Lower Cretaceous Saihan Formation serves as the main ore-bearing horizon. It is a coal-bearing clastic sequence rich in reducing agents such as organic matter and pyrite, primarily consisting of braided river, braided river delta, and shallow lacustrine deposits. The lithology is predominantly variegated, light yellow, and gray sandy conglomerates, conglomeratic sandstones, and sandstones, intercalated with thin layers of gray siltstone, mudstone, and coal seams (Figure 13C).

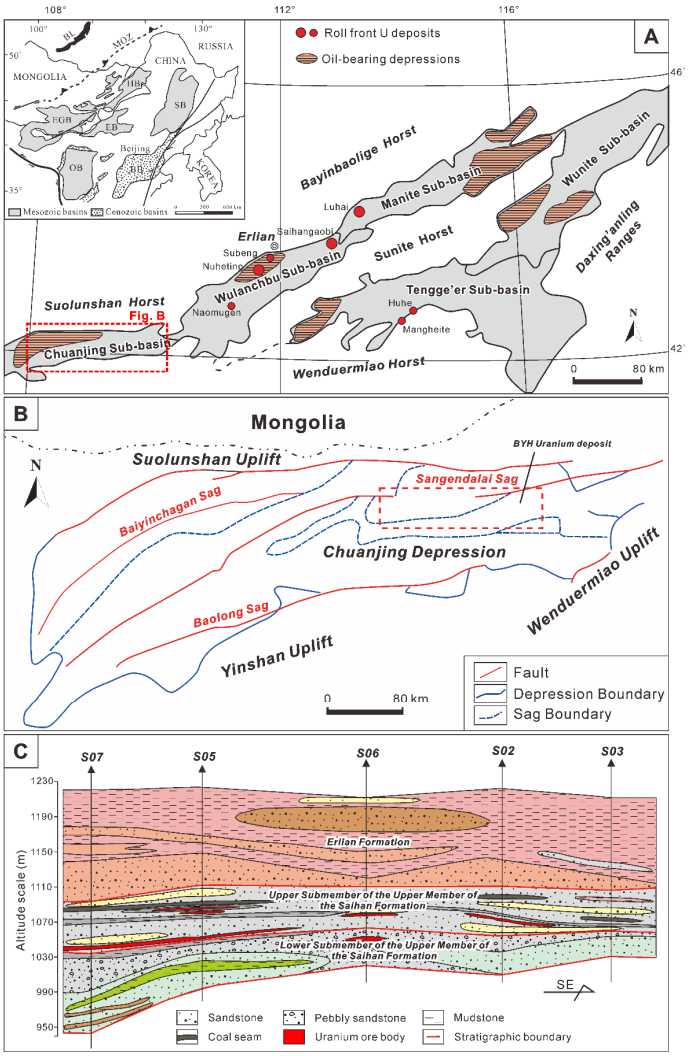

Figure 13. (**A**) Tectonic map of the Erlian Basin showing the distribution of different types of uranium deposits and oil-bearing sags, modified after [19]. BB = Bohai Basin, EB = Erlian Basin, EGB = East Gobi Basin, HB = Hailar Basin, OB = Ordos Basin, SB = Songliao Basin, YB = Yingen Basin, BL = Baikal Lake, MOZ = Mongol-Okhotsk Zone. (**B**) Tectonic division map of the Chuanjing Depression, modified after [17]. (**C**) SE–NW trending cross-section of sand bodies showing correlation between boreholes in the Sangendalai Sag, Chuanjing Depression, modified after [17].

4.4.1. Delineation of Oxidation-Reduction Zones

Zhu et al. (2025) [17] employed core spectral technology to conduct continuous measurements of ferric iron oxide content, constructing an NW-SE trending cross-section of variations in boreholes intersecting the Saihan Formation (Figure 14). This cross-section visually illustrates the lateral and vertical distribution patterns of iron oxides. Laterally, variations in iron oxide content primarily reflect paleotopographic relief during deposition and do not exhibit obvious pinch-out patterns. Notably, the distribution of iron oxides in the upper submember of the upper Saihan Formation member is relatively consistent. Vertically, however, the iron oxide content in the upper submember is significantly higher than that in the lower submember. Crucially, within zones of uranium orebody enrichment, iron oxide content decreases markedly, forming a distinct boundary of abrupt content change, while oxidation intensity increases in the upper part of the orebody (Figure 14). This spatial coupling between "low-value anomalies" in iron oxide content and uranium mineralization clearly delineates the precise location of the oxidation–reduction front. Based on these observations, the authors inferred that reduction intensity is slightly higher in the northwest compared to the southeast, and that epigenetic reduction intensity in the lower submember is stronger than in the upper submember.

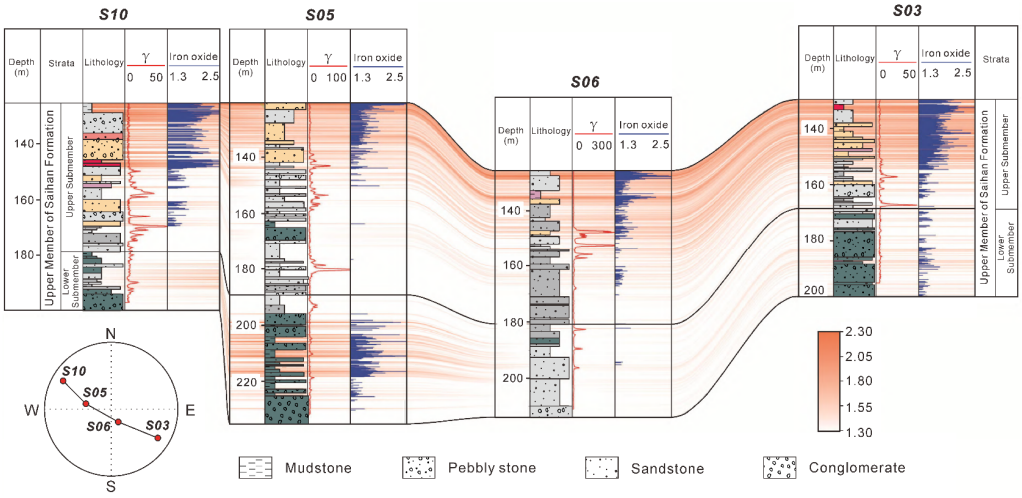

Figure 14. NW-SE trending cross-section showing ferric iron oxide content variations in boreholes intersecting the Saihan Formation in the Sangendalai Sag, Erlian Basin, modified after [17]. Spectral data were acquired using the CMS350A fully automated digital core scanner, jointly developed and introduced by the Nanjing Geological Survey Center, China Geological Survey, and the Nanjing Zhongdi Instrument Company. This cross-section visually illustrates the lateral and vertical distribution patterns of iron oxides. Laterally, variations in iron oxide content do not exhibit obvious pinch-out patterns. Notably, the distribution of iron oxides in the upper submember of the upper Saihan Formation member is relatively consistent. Vertically, the iron oxide content in the upper submember of the upper Saihan Formation member is significantly higher than that in the lower submember. Crucially, within zones of uranium orebody enrichment, iron oxide content decreases markedly, forming a distinct boundary of abrupt content change, while oxidation intensity increases in the upper part of the orebody. The color of the core column in the figure represents the color of the rock.

4.4.2. Tracing of Ore-Forming Fluids

Zhu et al. (2025) [17] suggested that the reduction intensity is slightly higher in the northwestern area compared to the southeastern area, and that the intensity of epigenetic reduction in the lower submember is stronger than that in the upper submember. Based on these observations, they further speculated that reducing fluids might have originated from the vertical escape of underlying hydrocarbon fluids. This demonstrates that even without

complex mineral assemblage identification, high-density, continuous measurements of a single mineral component (iron oxides) can effectively constrain oxidation–reduction zoning and help interpret fluid migration pathways.

4.5. Horizontal Comparison and Comprehensive Review

Comparing the four basin cases reveals different application strategies for core spectral technology in sandstone-type uranium deposits.

4.5.1. Differences in Alteration Mineral Assemblages

The Qianjiadian deposit is characterized by the antithetic relationship between kaolinite and montmorillonite, reflecting alternating acidic and alkaline fluids; the Yuejin-II deposit is characterized by coupled enrichment of the chlorite-carbonate assemblage, indicating spatial coupling of reducing fluids with an unconformity; the Pengyang deposit is characterized by a sharp increase in gypsum, reflecting oxidation of acidic hydrocarbon-bearing fluids; the Sangendalai Sag uses low-value anomalies of ferric iron oxides to delineate the oxidation–reduction front. These differences are primarily controlled by different fluid end-members (supergene oxygenated water vs. deep hydrocarbon-bearing fluids) and tectonic settings (unconformities, fault systems).

4.5.2. Different Technical Emphases

In deposits with well-defined alteration assemblages (e.g., Qianjiadian), SWIR is mainly used for detailed clay mineral mapping and fluid tracing; in deposits where mineralization is well-coupled with specific assemblages (e.g., Yuejin-II), SWIR can delineate layered alteration zones and trace orebody extensions; in deposits with clear oxidation–reduction zoning (e.g., Sangendalai), SWIR can quickly locate the front using single-mineral (iron oxide) content measurements; in deep-seated concealed deposits (e.g., Pengyang), SWIR helps reconstruct fluid properties and metallogenic environments.

4.5.3. Implications for Applicability

These cases indicate that successful application of SWIR in sandstone-type uranium deposits depends on a thorough understanding of the deposit's geological background. Prioritizing mining areas with abundant alteration minerals, relatively homogeneous lithology, and weak post-mineralization modification can improve the accuracy and reliability of spectral interpretation.

5. Challenges and Prospects

5.1. Instrumental and Spectral Limitations and Response Strategies

5.1.1. Instrumental and Spectral Limitations

The key to interpreting spectral data is to understand the variables that influence spectra. Multiple variables can affect spectral results, including grain size, transparency, sulfide content, overall reflectance, water content, heavy metals, contaminants (e.g., grease, organic matter), mineral orientation, and degree of mineral mixing [65]. Grain size primarily affects light scattering and absorption paths. Coarser grains enhance scattering, increasing overall reflectance but potentially masking absorption features. Finer grains may make absorption features more pronounced. Increased surface roughness can cause "shadowing effects," reducing the signal-to-noise ratio [66]. Transparent minerals (e.g., quartz) allow light to penetrate, causing multiple internal reflections that may enhance or obscure absorption features. Opaque minerals (e.g., sulfides) are dominated by surface reflectance and may mask SWIR signals. The spectra of translucent minerals (e.g., chlorite, illite) are influenced by thickness [67]. Sulfides such as pyrite (Fe-S bonds) lack SWIR-active chemical bonds

(OH^-, H_2O, CO_3^{2-}, NH_4^+), with absorption peaks mainly in the mid- to far-infrared (>2500 nm) [68], beyond the detection range of core spectral technology. Moreover, pyrite's metallic luster can generate strong specular reflection, masking the SWIR absorption signals of surrounding alteration minerals. Therefore, during measurement, areas with widespread pyrite should be avoided as much as possible. Organic matter (humic acids, kerogen, bitumen, grease) has its own distinct absorption features in the SWIR region due to C-H vibrations (1720–1750 nm, 2300–2350 nm, and 1400/1900 nm) [39], which may overlap with characteristic features of clays and carbonates. In practical applications, however, most sandstone-type uranium deposits in northern China are characterized by the coexistence of oil and uranium, so organic matter is not considered an interfering factor. On the contrary, its strong absorption can be leveraged to identify hydrocarbons and evaluate reducing capacity. The degree of mineral mixing is also a key factor affecting identification accuracy. Physical mixing (e.g., quartz + clay) can dilute absorption depths, while chemical mixing (e.g., I/S mixed layers) can cause peak shifts or broadening. Additionally, the wavelength range of this technology is not suitable for identifying most anhydrous silicate minerals. When the mineral content is below 5%, identification using this technology is generally difficult, unless the sample is a simple binary mixture with a spectrally neutral matrix like quartz, and the target mineral has a high albedo. However, as a general rule, mineral content needs to reach 10% or more for definitive determination. If the sample contains minerals with low reflectance (e.g., carbonates, chlorite), identification may require even higher mineral contents [65].

5.1.2. Response Strategies for Instrumental and Spectral Limitations

In response to the instrumental and spectral limitations outlined in Section 5.1.1, the following practical strategies are proposed for sandstone-type uranium deposits, taking into account their specific lithological and mineralogical characteristics.

Multi-Scale Measurement and Normalization

Given the strong heterogeneity of grain size and the common interbedding of sandstones and mudstones in sandstone-type uranium deposits, a single-point measurement can hardly represent the true spectral characteristics of the sample. To reduce errors caused by grain-size variations and surface roughness, it is recommended to: (1) Take measurements at multiple points on the same sample and calculate the average reflectance spectrum. (2) Use a contact probe with a larger spot size (e.g., >1 cm diameter) to integrate signals from a broader area. (3) Normalize spectra using continuum removal to enhance subtle absorption features and facilitate comparison between different lithologies.

Avoidance of Pyrite Interference

Pyrite is commonly associated with uranium mineralization in sandstone-type deposits. Its metallic luster generates strong specular reflection, which can mask SWIR absorption signals of surrounding alteration minerals (such as illite and chlorite). Effective mitigation strategies include: (1) Identify pyrite-rich zones by visual inspection or core scanning images before measurement and avoid these areas during data acquisition. (2) Applying post-processing algorithms to detect and remove high-reflectance outliers caused by specular reflection. (3) Using coarser spectral sampling intervals or spatial filtering to reduce the influence of isolated pyrite grains

Utilization of Organic Matter

In many sandstone-type uranium deposits of northern China, particularly oil-bearing basins such as the Qaidam Basin, organic matter and hydrocarbons are closely associated with uranium mineralization. Although organic matter can interfere with the identifica-

tion of clay and carbonate minerals due to overlapping absorption features (e.g., C–H bonds around 1730 nm and 2310 nm), it also represents a valuable indicator of reducing conditions. Practical strategies include: (1) Using characteristic hydrocarbon absorptions at 1730 nm and 2310 nm as direct proxies for the presence of reductants. (2) Evaluating reduction capacity by calculating the absorption depth ratio of these hydrocarbon bands. (3) Incorporating organic matter absorption intensity as an auxiliary parameter in redox environment characterization.

Spectral Unmixing Strategies

Mineral mixing is a common issue in sandstone-type uranium deposits, occurring both as physical mixtures (e.g., quartz + clay) and chemical mixtures (e.g., illite-smectite mixed layers). To improve the accuracy of mineral identification and semi-quantitative estimation, the following approaches are recommended: (1) For physical mixtures: apply linear spectral unmixing algorithms (e.g., LSMM) to separate endmember spectra and estimate their relative abundances. (2) For chemical mixtures (e.g., I/S mixed layers): rely on changes in FWHM and absorption peak positions (e.g., the 1900 nm H_2O feature and 2200 nm Al-OH feature) to infer mixing ratios. (3) For low-reflectance minerals (e.g., carbonates, chlorite), supplementary analytical methods such as XRD should be used to validate SWIR results, especially when mineral content is near or below the detection limit (~10%).

5.2. Geological Complexity and Identification Methods

5.2.1. Geological Complexity

Currently, core spectral technology (particularly SWIR) has been widely applied in mineral exploration, successfully establishing prospecting indicators for various deposit types [69–86], especially magmatic–hydrothermal deposits. However, applying this technology to sandstone-type uranium deposits presents distinct challenges due to fundamental differences in host rock lithology, alteration mineral assemblages, fluid properties, and, most importantly, the interpretive framework for spectral data.

Fundamental Differences

In magmatic–hydrothermal systems (e.g., porphyry Cu deposits), alteration minerals typically form concentric, ring-like zonation patterns around a fluid source, providing a clear spatial vector to mineralization [33,34,71,80,85,86]. These deposits have homogeneous igneous or metamorphic host rocks (granite, andesite, tuff), where primary minerals (quartz, feldspar, amphibole) exhibit weak or no SWIR response, making hydrothermal alteration minerals (illite, kaolinite, alunite) easily identifiable [33,65]. In contrast, sandstone-type uranium deposits are hosted in interbedded sandstone–mudstone sequences. Alteration is controlled by facies architecture, redox interfaces, and permeability contrasts, resulting in irregular, stratigraphically controlled patterns. Rapid lithological variations cause poor vertical continuity of SWIR data [8], and alteration minerals are easily confused with detrital or diagenetic phases (e.g., clay minerals from montmorillonite-to-illite transformation) [87]. The ore-forming fluids are typically low-temperature oxidation–reduction fluids (meteoric or basinal brines), and uranium grades are relatively low. Consequently, spectral parameters used for magmatic–hydrothermal systems (e.g., chlorite Pos2250 shifts, IC values, and Pos2200 values) [33–35,75,76,88–90] do not exhibit significant changes in sandstone-type deposits. A concise comparison of key characteristics is provided in Table 1.

Table 1. Comparison of key characteristics between sandstone-type uranium deposits and magmatic–hydrothermal deposits in hyperspectral applications.

Aspect	Sandstone-Type U Deposit	Magmatic–Hydrothermal Deposit (e.g., Porphyry Cu)
Host rock lithology	Interbedded sandstone–mudstone, complex, rapidly changing	Homogeneous igneous/metamorphic rock
Alteration mineral assemblage	Low-T: kaolinite, smectite, illite, chlorite, carbonate, pyrite	High-T: K-feldspar, biotite, sericite, alunite, pyrophyllite
Alteration zoning	Irregular, stratabound oxidation–reduction zones	Regular, concentric areal alteration zones
Ore-forming fluid	Low-T (<120 °C), redox (meteoric/basinal brine + hydrocarbons)	High-T (>200 °C), acidic hydrothermal
Spectral prospecting indicators	Appearance/disappearance of assemblages, relative abundance changes, Fe-oxide low anomalies [91,92]	Peak shifts (e.g., Pos1480, Pos2200, Pos2250), IC values [33,34,75,76,88]
Technical focus	Locating redox fronts, distinguishing fluid end-members, separating alteration from diagenetic background	Tracing hydrothermal centers, mapping alteration zones, targeting exploration
Main challenges	Diagenetic mineral interference, weak low-T signals, rapid lithological changes	Overprinting alteration, erosion level assessment

Implications for SWIR Application

The above differences necessitate a shift in interpretive framework when applying SWIR in sandstone-hosted systems. In hydrothermal deposits, the goal is "zonation vectoring" toward a heat/fluid source [33,34,85,86]. In sandstone-type deposits, the goal is "facies and redox mapping" to locate oxidation–reduction fronts and identify favourable fluid mixing zones. Therefore, successful application of SWIR in sandstone-type uranium deposits requires a preliminary understanding of the regional fluid system (e.g., meteoric, hydrocarbon, basinal brine) [91,92] to interpret which alteration assemblages are likely mineralization-related versus diagenetic [87]. For example, Ghoneim et al. (2023) demonstrated that in the El Sela area, successive hydrothermal alterations (beresitization, propylitization, argillitization) along shear zones were key to uranium remobilization, and understanding these fluid–rock interactions allowed effective use of radiometric and mineralogical data to distinguish mineralized zones [93]. This principle applies equally to SWIR-based alteration studies: without knowing the dominant fluid end-members, spectral patterns cannot be reliably assigned to mineralization.

In summary, sandstone-type uranium deposits should not be explored using the same SWIR approach as magmatic–hydrothermal systems. Exploration geologists should shift from "zonation vectoring" to "facies and redox mapping" when applying SWIR in sandstone-hosted systems [33,34,65,87]. This conceptual takeaway is essential for maximizing the value of spectral data in these deposits.

5.2.2. Response Strategies for Geological Complexity

Criteria for Distinguishing Syn-Mineralization Alteration from Diagenetic Background

(1) Spatial correlation: syn-mineralization alteration is typically spatially associated with uranium mineralization intervals (high gamma-ray anomalies), while diagenetic minerals have wider distribution with no correlation. (2) Assemblage characteristics: syn-mineralization alteration often forms specific assemblages (e.g., chlorite + carbonate + pyrite [8]), while diagenetic assemblages are simpler. (3) Microtextural evidence: pet-

rographic observation shows syn-mineralization alteration occurs as pore-filling cements or replaces precursor minerals, whereas diagenetic minerals occur as detrital grains or early cements.

Dealing with Rapid Lithological Variations

In intervals with complex lithology (e.g., interbedded mudstone and sandstone), establish background baselines for each lithology separately and extract anomalies by difference; or focus on relatively homogeneous sandstone intervals and avoid mudstone-dominated sections.

Spectral Proxies for Low-Temperature Systems

Since sandstone-type uranium deposits have low formation temperatures (<120 °C), traditional high-temperature spectral proxies (e.g., chlorite Pos2250 shifts) are not applicable. Instead, focus on qualitative to semi-quantitative indicators such as the appearance/disappearance of mineral assemblages (e.g., disappearance of iron oxides) and relative changes in mineral abundance (e.g., increased chlorite absorption depth).

5.3. Interpretational Pitfalls and Future Directions

5.3.1. Interpretational Pitfalls to Avoid

Based on the practical experience gained from the four typical sandstone-type uranium deposits reviewed in this study, several interpretational pitfalls should be carefully avoided when applying SWIR technology.

Avoid Over-Reliance on Single Mineral Indicators

Although kaolinite enrichment shows a good spatial correlation with uranium mineralization in the Qianjiadian deposit, this relationship is not universal. In other basins, kaolinite may simply reflect diagenetic acidification unrelated to uranium mineralizing events. Therefore, it is recommended to: (1) Integrate multiple mineral parameters (kaolinite, montmorillonite, illite, iron oxides, carbonates) in the interpretation. (2) Pay attention to mineral assemblages (e.g., kaolinite + pyrite + ankerite in the oxidation-reduction transition zone) rather than individual mineral anomalies.

Use Spectral Parameter Shifts Cautiously

In magmatic-hydrothermal systems, systematic shifts in spectral parameters such as the Pos2200 value of illite or the Pos2250 value of chlorite are frequently used as vectors toward mineralization centers. However, in low-temperature sandstone-type uranium deposits (T < 120°C), these spectral parameters generally do not show significant variations. Thus, it is not appropriate to directly transplant these high-temperature spectral proxies. Instead, priority should be given to: (1) The presence or absence of diagnostic mineral assemblages. (2) Relative changes in mineral abundances (e.g., absorption depth increases in chlorite or carbonates [8]). (3) The spatial relationship between specific mineral associations and uranium mineralization intervals.

Necessity of Multi-Method Validation

SWIR is an excellent tool for rapid screening of alteration minerals over long core intervals, but it has limitations in identifying low-abundance minerals (typically <5%–10%) and cannot reliably distinguish syn-mineralization alteration from background diagenetic alteration. Therefore, SWIR results should always be validated by: (1) Petrographic observations (optical microscopy, BSE imaging). (2) Electron probe microanalysis (EPMA) for mineral chemistry, especially for critical minerals like chlorite and carbonates. Such

a multi-method approach ensures the accuracy and reliability of mineral identification and interpretation.

5.3.2. Future Directions

Multi-Method Integration

A systematic workflow is proposed for future research: (1) SWIR rapid scanning over long core intervals, (2) targeted sampling based on key spectral anomalies, (3) petrographic validation, (4) XRD and EPMA quantification, (5) comprehensive interpretation integrating mineralogical and spectral data.

Intelligent Data Processing

The application of machine learning algorithms (e.g., random forest, convolutional neural networks) for automatic mineral identification and spectral unmixing is a promising direction. Training models on large datasets of SWIR spectra with corresponding XRD and thin-section labels can significantly improve the accuracy and efficiency of mineral mapping.

Quantitative Models

Build calibration models between mineral content and spectral parameters specifically for sandstone-type uranium deposits. Establishing quantitative relationships between spectral parameters (such as absorption depth and FWHM) and mineral abundance under controlled conditions is essential for advancing from semi-quantitative to quantitative SWIR applications.

3D Modeling

By integrating SWIR data from multiple boreholes, 3D models of alteration mineral distribution can be constructed. These models can visualize the spatial morphology of oxidation-reduction fronts and guide further drilling and resource estimation.

Standardization

Establish industry technical standards covering data acquisition, processing, and interpretation workflows. Industry-wide technical standards are urgently needed to ensure data comparability across different instruments and projects.

6. Conclusions

(1) Applicable conditions: Core spectral technology (especially SWIR) is suitable for sandstone-type uranium mining areas with abundant alteration minerals (target mineral content > 5%–10%), relatively homogeneous lithology or strategies to overcome heterogeneity, and clear spatial coupling between alteration and mineralization. Priority should be given to deposits developing SWIR-sensitive minerals such as chlorite, carbonate, kaolinite, illite, and iron oxides.

(2) Key prospecting indicators: Mineral assemblage indicators include: oxidation zone marked by "kaolinite + Fe^{3+} oxides"; reduction zone marked by "montmorillonite + illite + pyrite"; transition zone marked by "kaolinite + montmorillonite + pyrite + ankerite" or "chlorite + carbonate". Single-mineral content indicators include sharp increases in chlorite or carbonate absorption depth, or significant decreases in ferric iron oxide absorption depth, can serve as indirect indicators of mineralization intervals. Specific mineral anomalies include sharp increases in gypsum (e.g., Pengyang) or the antithetic relationship between kaolinite and montmorillonite (e.g., Qianjiadian) can indicate fluid properties. The applicability of these indicators is basin-specific.

(3) Main limitations: Detection limit (difficult to identify when alteration mineral content is <5%–10%), lithological interference (interbedded sandstone–mudstone sequences lead to poor vertical continuity of spectral signals), mineral confusion (syn-mineralization alteration easily confused with diagenetic background), low-temperature limitation (not suitable for heat-source tracing based on spectral parameter shifts), and spectral masking by opaque minerals such as pyrite.

(4) Future directions: Multi-method integration (establish a workflow of "SWIR rapid mapping—petrographic validation—XRD/EPMA precise quantification"), intelligent data processing (develop machine learning-based automatic mineral identification and spectral unmixing algorithms), quantitative models (establish calibration models between mineral content and spectral parameters), 3D modeling (construct deposit-scale 3D alteration models), and standardization (establish industry technical standards).

(5) Application prospects: The integrated application of core spectral technology with petrography, XRD, SEM, and electron probe microanalysis holds considerable promise for advancing metallogenic research and prospecting practices for sandstone-type uranium deposits in northern China.

Author Contributions: Conceptualization, W.W., M.F. and P.N.; Methodology: W.W., M.F. and P.N.; Investigation: W.W., J.P., Y.L., Z.C. and J.D.; Data curation: W.W., Y.L. and Z.C.; Writing—original draft preparation: W.W. and M.F.; Writing—review and editing: M.F., P.N., J.P., Y.L. and J.D.; Visualization: W.W. and Y.L.; Supervision: P.N. and M.F.; Project administration: P.N., M.F. and J.P.; Funding acquisition: P.N. All authors have read and agreed to the published version of the manuscript.

Funding: This research was funded by the National Key Research and Development Program of China (Grant No. 2023YFC2906703).

Data Availability Statement: Not applicable.

Acknowledgments: We sincerely thank the Exploration Division of PetroChina Qinghai Oilfield Company and the 11th Geological Brigade of Sichuan Province for their assistance during our fieldwork in the Qigequan and Yuejin-II areas of the Qaidam Basin. We thank Yu-Guan Pan and Yuan-Feng Cai from Nanjing University for their support with X-ray diffraction (XRD) analysis. We also thank Hao-Ran Dou from Nanjing Hongchuang Geological Exploration Technology Service Co., Ltd. for his assistance with backscattered electron (BSE) imaging and electron probe microanalysis (EPMA). We acknowledge the technical support provided by Fei-Peng Fan and Yan Zhou from the Nanjing Center of the China Geological Survey regarding short-wave infrared (SWIR) spectral analysis. This study was supported by the National Key Research and Development Program of China (Grant No. 2023YFC2906703).

Conflicts of Interest: The authors declare no conflicts of interest. The funders had no role in the design of the study; in the collection, analyses, or interpretation of data; in the writing of the manuscript; or in the decision to publish the results.

References

1. NEA. *Uranium 2022: Resources, Production and Demand*; OECD Publishing: Paris, France, 2023.
2. Yan, Q.; Wang, A.J.; Wang, G.S.; Yu, W.J.; Chen, Q.S. Research on nuclear power development strategy. *Forum Sci. Technol. China* **2009**, *26*, 18–22. (In Chinese)
3. Li, Q.; Chen, Q.; Wang, J.B.; Chen, Y.J.; Kang, L.G.; Chen, B.; Shi, Z.H. Current situation of uranium resources in the world and suggestions on resource guarantee of nuclear power development in China. *China Min. Mag.* **2023**, *32*, 1–9. (In Chinese)
4. Jin, R.S.; Zhang, C.J.; Feng, X.X.; Tao, C.; Zhu, Q.; Li, G.Y. The influence of fluid mixing on the mineralization of sandstone type uranium deposits. *Geol. Bull. China* **2013**, *33*, 354–358. (In Chinese)
5. Chen, L.L.; Nie, F.J.; Yan, Z.B.; Feng, Z.B.; Liu, J.; Li, X.D. The Analysis of Basin-mountain Evolution and Sandstone-type Uranium Mineralization of Meso-Cenozoic U-producyive Basins in Northern China. *Sci. Technol. Eng.* **2014**, *14*, 163–170. (In Chinese)
6. Fu, Y.; Wei, S.C.; Jin, R.S.; Li, J.G.; Ao, C. Current status and existing problems of China's sandstone-type uranium deposits. *Acta Geol. Sin.* **2016**, *90*, 3519–3544. (In Chinese)

7. Lin, Y.-H.; Fan, M.-S.; Ni, P.; Pan, J.-Y.; Jin, R.-S.; Cheng, Y.-H.; Cui, J.-M.; Cheng, Z.-L.; Li, W.-S.; Zhu, Q.; et al. New insights into uranium source and mineralization process of the world-class jingchuan sandstone-hosted uranium deposit, ordos basin, China: Evidence from geology, carbonate textures and geochemistry. *Ore Geol. Rev.* **2025**, *185*, 106795. [CrossRef]
8. Wu, W.Y.; Fan, M.S.; Ni, P.; Pan, J.Y.; Lin, Y.H.; Zhou, Y.; Zhang, C.; Shi, R.Y.; Gao, X.F.; Wang, D.; et al. Application of short-wave infrared spectroscopy in sandstone-type uranium deposits: A case study of the Yuejin-II uranium deposit in the Qaidam Basin, China. *J. Geochem. Explor.* **2026**, *286*, 108041. [CrossRef]
9. Cheng, Y.H.; Zhang, T.F.; Zeng, W.; Hu, P.; Liu, X.; Yang, J.; Qu, K.; Wang, S.Y.; Cheng, X.Y.; Ao, C.; et al. Driving Forces for Sandstone-type Uranium Super-enrichment in Meso-Cenozoic Basins, North China. *Geotecton. Metallog.* **2020**, *44*, 590–606. (In Chinese)
10. Miao, P.S.; Chen, Y.; Cheng, Y.H.; Zhao, H.L.; Chen, L.L.; Li, J.G.; Jin, R.S.; Tang, C.; Yu, R.A.; Yang, T.; et al. New Deep Exploration Discoveries of Sandstone-type Uranium Deposits in North China. *Geotecton. Metallog.* **2020**, *44*, 563–575. (In Chinese)
11. Xing, X.J.; Liu, Y.Q.; Li, W.H.; Gong, B.L. Sandstone Diagenesis and Uranium Mineralization of the Zhiluo Formation in the Diantou Area Southern Ordos Basin. *Acta Geosci. Sin.* **2008**, *29*, 179–188. (In Chinese)
12. Miao, P.S.; Zhang, B.; Zhang, H.L.; Li, J.G.; Lu, Y.; Ao, C.; Cao, M.Q.; Xue, L.; Xuan, Y.S. Automated drill core spectral scanning technique in the study of altered minerals in sandstone-type uranium deposits. *N. China Geol.* **2017**, *40*, 210–218. (In Chinese)
13. Li, J.G.; Zhang, B.; Jin, R.S.; Si, Q.H.; Miao, P.S.; Li, H.L.; Cao, M.Q.; Wei, J.L.; Chen, Y. Uranium Mineralization of Coupled Supergene Oxygen-Uranium Bearing Fluids and Deep Acidic Hydrocarbon Bearing Fluids in the Qianjiadian Uranium Deposit, Kailu Basin. *Geotecton. Metallog.* **2020**, *44*, 576–589. (In Chinese)
14. Zhang, B.; Si, Q.H.; Miao, P.S.; Zhao, H.L.; Zhu, Q.; Chen, Y.; Chen, L.L. Mineral Distribution Characteristics of the Pengyang Uranium Deposit Based on Near Infrared Core Spectral Scanning Technology. *Rock Miner. Anal.* **2022**, *41*, 733–743. (In Chinese)
15. Huang, S.H.; Liu, Z.Y.; Qin, M.K.; He, Z.B. Metallogenic Environment of Sandstone-Hosted Uranium Deposit Based on Portable Colorimeter, X-ray Spectrofluorometer and Hyperspectrometer: Taking the Telaaobao Uranium Deposit in Northwestern Ordos Basin as An Example. *Geol. Explor.* **2023**, *59*, 1182–1193. (In Chinese)
16. Zhang, Y.T. Research on Lithology Identification Technology for Sandstone Uranium Ore Cores Using Imaging Spectroscopy. Ph.D. Thesis, Beijing Research Institute of Uranium Geology, Beijing, China, 2023. (In Chinese)
17. Zhu, Q.; Si, Q.H.; Wen, S.B.; Yu, R.A.; Li, G.Y.; Zhang, B.; Wang, S.B.; Peng, S.L.; Li, J.M. Petrological and Mineralogical Characteristics of the Saihan Formation in the Sanggendalai Sag of the Erlian Basin and Their Indications for Uranium Enrichment. *Acta Geosci. Sin.* **2025**, *46*, 456–470. (In Chinese)
18. Lin, Y.H.; Fan, M.S.; Ni, P.; Pan, J.Y.; Chi, Z.; Cheng, Z.L.; Wu, W.Y.; Zhang, C.; Qi, B.D.; Wei, X.B. A novel mechanism of uranium mineralization: The role of zircon adsorption at the Qigequan deposit, Qaidam Basin, NW China. *Sediment. Geol.* **2026**, *493*, 107027. [CrossRef]
19. Bonnetti, C.; Cuney, M.; Malartre, F.; Michels, R.; Liu, X.; Peng, Y. The nuheting deposit, erlian basin, NE China: Synsedimentary to diagenetic uranium mineralization. *Ore Geol. Rev.* **2015**, *69*, 118–139. [CrossRef]
20. Merriman, R. Contrasting caly mineeral assemblages in British Lower Palaeozoic slate belts: The influence of geotectonic setting. *Clay Miner.* **2002**, *37*, 207–219. [CrossRef]
21. Deconinck, J.F.; Blanc-Valleron, M.; Rouchy, J. Palaeoenviron- mental and diagenetic control of the mineralogy of Upper Cretaceous-lower tertiary deposits of the central palaeo-andean basin of Bolivia (Potosi area). *Sediment. Geol.* **2000**, *132*, 263–278. [CrossRef]
22. Perederij, V.I. Clay mineral composition and palaeoelimatic interpretation of the Pleistocene deposits of Ukraine. *Quat. Int.* **2001**, *76*, 113–121. [CrossRef]
23. Li, J.G.; Jin, R.S.; Zhang, B.; Miao, P.S.; Yang, K.; Li, H.L.; Wei, J.L.; Ao, C.; Cao, M.Q.; Zhang, H.L.; et al. Characteristics of Primary Clay Minerals in the Upper Cretaceous Yaojia Formation of Southwest Songliao Basin and Their Significance. *Acta Geosci. Sin.* **2018**, *39*, 295–305. (In Chinese)
24. Li, W.T.; Li, Z.Y.; Li, X.D.; Liu, W.S.; Kang, S.H.; Lyu, Y.H. The Characteristics of Clay Mineral and Its Relationship to Uranium Mineralization in Hadatu Uranium Deposit, Erlian Basin. *Uranium Geol.* **2020**, *36*, 96–103. (In Chinese)
25. Li, H.M.; Li, L.; Peng, Y.B.; Yan, P.B.; Yi, C. Study on the relationship between clay minerals and genesis of oxidation zone of sandstone uranium deposits, northern Ordos Basin. *Chin. J. Geol.* **2021**, *56*, 303–320. (In Chinese)
26. Shan, Z.B.; Lei, A.G.; Song, B.R.; Ao, C.; Yang, S.L.; Han, H.D. Features of clay minerals in the Upper Cretaceous Yaojia Formation sandstones of the Qianjiadian Area in the Songliao Basin and its relation to uranium mineralization. *Geol. China* **2022**, *49*, 271–283. (In Chinese)
27. Zang, Y.H.; Ning, J.; Wang, C.D.; Dong, X.Y.; Zhang, L.L.; Lu, T.J.; Yan, Z.B. Study on alteration mineral characteristics of Yaojia Formation sandstone and its relationship with uranium mineralization in Hailijin uranium deposit, southern Songliao Basin. *Miner. Depos.* **2026**, *45*, 189–208. (In Chinese)
28. Zhao, J.Q.; Dong, X.F.; Li, N.; Yan, B.K.; Gan, F.P.; Wang, W.D.; Lu, C.L. Alteration characteristic and prospecting prediction of the Huaxishan gold deposit in Gansu Province based on hyperspectral data. *Geol. Explor.* **2023**, *59*, 122–133. (In Chinese)

29. Oluwadebi, A.G.; Hecker, C.A.; Meer, F.D.V.D.; Ferrier, G. Mapping of hydrothermal alteration in mount berecha area of main ethiopian rift using hyperspectral data. *J. Environ. Earth Sci.* **2013**, *3*, 115–124.
30. Cao, F.S. Rapid Evaluation Method of Ore Deposits Based on Portable XRF and Hyperspectral. Ph.D. Thesis, Chengdu University of Technology, Chengdu, China, 2021; pp. 3–131. (In Chinese)
31. Zhang, J.L.; Huang, Y.J.; Wang, J.H.; Zhou, M.; Wu, D.; Xuan, Y.X. Hyperspectral drilling core logging and 3D mineral mapping technology for uranium exploration. *Uranium Geol.* **2013**, *29*, 249–255. (In Chinese)
32. Herrmann, W.; Blake, M.; Doyle, M.; Huston, D.; Kamprad, J.; Merry, N.; Pontual, S. Short Wavelength Infrared (SWIR) Spectral Analysis of Hydrothermal Alteration Zones Associated with Base Metal Sulfide Deposits at Rosebery and Western Tharsis, Tasmania, and Highway-Reward, Queensland. *Econ. Geol.* **2001**, *96*, 939–955. [CrossRef]
33. Chang, Z.S.; Hedenquist, J.W.; White, N.C.; Cooke, D.R.; Roach, M.; Deyell, C.L.; Garcia, J., Jr.; Gemmell, J.B.; McKnight, S.; Cuison, A.L. Exploration Tools for Linked Porphyry and Epithermal Deposits: Example from the Mankayan Intrusion-Centered Cu-Au District, Luzon, Philippines. *Econ. Geol.* **2011**, *106*, 1365–1398. [CrossRef]
34. Yang, Z.M.; Hou, Z.Q.; Yang, Z.S.; Qu, H.C.; Li, Z.Q.; Liu, Y.F. Application of short wavelength infrared (SWIR) technique in exploration of poorly eroded porphyry Cu district: A case study of Niancun ore district Tibet. *Miner. Depos.* **2012**, *31*, 699–717. (In Chinese)
35. Qiu, J.H.; Liu, W.Y.; Chen, J.W.; Lai, X.D.; Zhong, X.H.; Li, J.; Long, H. Alteration mineralogy, characteristics and shortwave infrared spectroscopy of white mica in the Zijinshan ore field, Fujian Province: Implications for porphyry Cu prospecting. *Ore Geol. Rev.* **2024**, *168*, 106065. [CrossRef]
36. Hunt, G.R.; Salisbury, J.W. Visible and near-infrared spectra of minerals and rocks: I Silicate minerals. *Mod. Geol.* **1970**, *1*, 283–300.
37. Hunt, G.R.; Salisbury, J.W.; Lenhoff, G.J. Visible and near-infrared spectra of minerals and rocks: VI Additional silicate minerals. *Mod. Geol.* **1974**, *4*, 331–363.
38. Hunt, G.R. Spectral Signature of Particular Minerals, in the Visible and Infrared. *Geophysics* **1977**, *42*, 501–513. [CrossRef]
39. Clark, R.N.; Roush, T.L. Reflectance spectroscopy: Quantitative analysis techniques for remote sensing applications. *J. Geophys. Res. Solid Earth* **1984**, *89*, 6329–6340. [CrossRef]
40. Clark, R.N.; Swayze, G.A.; Wise, R.; Livo, K.E.; Hoefen, T.; Kokaly, R.F.; Sutley, S.J. *USGS Digital Spectral Library Splib06a*; USGS: Reston, Herndon, VA, USA, 2007.
41. Gan, F.P. *Theory and Technical Methods for Extracting Rock and Mineral Information from Remote Sensing Data*; Geological Publishing House: Beijing, China, 2004; pp. 56–57. (In Chinese)
42. Xiu, L.C.; Zheng, Z.Z.; Yu, Z.K.; Huang, J.J.; Yin, L.; Wang, M.J.; Zhang, Q.N.; Huang, B.; Chen, C.X.; Xiu, T.J.; et al. Mineral analysis technology application with Near Infrared Spectroscopy in identifying alteration mineral. *Acta Geol. Sin.* **2007**, *81*, 1584–1590. (In Chinese)
43. Guo, H.Y. Application of Rocks and Minerals Mapping Based on Hyperspectral Remote Sensing in Dongkunlun Nachitai. Master's Thesis, Chengdu University of Technology, Chengdu, China, 2009. (In Chinese)
44. Zhang, G. Application Study of SWIR Mineral Mapping at the Tuwu, Qulong and Pulang Copper Prospects, China. Ph.D. Thesis, China University of Geosciences, Beijing, China, 2005. (In Chinese)
45. Yang, K.; Cardy, M.; Mason, P.; Davey, C.; Roche, B.; Wilford, J.; Cudahy, T.; Thomas, M.; White, A.; Brown, S.; et al. *HyLogging for Characterisation of Clay Minerals and Carbonic in Drillhole Samples of the Yeelirrie Uranium Deposit*; CSIRO Report EP101859; CSIRO: Perth, WA, USA, 2010; p. 16.
46. Yang, K.; Huntington, J.F.; Quigley, M.; Whitbourn, L. Zonation of Clays in the Bowdens Ag-Pb-Zn Deposit, New South Wales: Implications for Mineral Exploration. In *Proceedings of SEG 2012*; SEG: Lima, Peru, 2012; pp. 26–28.
47. Lu, Y. Applications of Hyperspectral Mineral Mapping in Mineral and Petroleum Exploration. Ph.D. Thesis, China University of Geosciences, Beijing, China, 2018. (In Chinese)
48. Zhang, C.; Ye, F.W.; Wang, J.G.; Qiu, J.T.; Meng, S. Spectral Characteristics Analysis of Drill Core in the Xiangyangping Uranium Deposit in the Middle Miaoershan Mountain, Northeastern Guangxi. *Uranium Geol.* **2019**, *35*, 366–374. (In Chinese)
49. Ding, B.; Liu, H.X.; Xu, D.R.; Qiu, L.F.; Zhang, Z.L.; He, F. Uranium Metallogenic Effect of Hydrothermal Fluid Transformation in Sandstone-Type Uranium Deposits in Northern Ordos Basin: Constraints from the Study of Biotite Chloritization Process. *Earth Sci.* **2024**, *49*, 625–638. (In Chinese)
50. Cloutis, E.A. Spectral reflectance properties of hydrocarbons: Remote-sensing implications. *Science* **1989**, *245*, 165–168. [CrossRef]
51. Clark, R.N.; King, T.V.V.; Klejwa, M.; Swayze, G.A.; Vergo, N. High spectral resolution reflectance spectroscopy of minerals. *J. Geophys. Res.* **1990**, *95*, 12653–12680. [CrossRef]
52. Allen, C.S.; Krekeler, M.P.S. Reflectance spectra of crude oils and refined petroleum products on a variety of common substrates. In *Proceedings of the SPIE Defense, Security, and Sensing, Orlando, FL, USA, 5–9 April 2010*; SPIE: Bellingham, WA, USA, 2010; Volume 7687, pp. 61–64.
53. Huang, S.J. Formation conditions and prospecting criteria for sandstone uranium deposit of interlayered oxidation type. *Uranium Geol.* **1994**, *10*, 6–13. (In Chinese)

54. Cheng, F.; Jolivet, M.; Guo, Z.J.; Wang, L.; Zhang, C.H.; Li, X.Z. Cenozoic evolution of the Qaidam basin and implications for the growth of the northern Tibetan plateau: A review. *Earth-Sci. Rev.* **2021**, *220*, 103730. [CrossRef]
55. Jin, R.S.; Zhu, Q. Supernormal enrichment mechanism and metallogenic process of sandstone type uranium deposit in the eolian sedimentary system in Jingchuan area. *Ordos Basin. Acta Geol. Sin.* **2023**, *97*, 725–737. (In Chinese)
56. Han, X.Z.; Wu, Z.J.; Sima, X.Z.; Yu, R.A.; Li, J.; Hu, H.; Jiang, Z. Metallogenic model of uranium with source supply from the south and the north in Manite depression of Erlian basin, Inner Mongolia. *Coal Geol. Explor.* **2018**, *46*, 1–10. (In Chinese)
57. Nie, F.J.; Yan, Z.B.; Feng, Z.B.; Li, M.; Xia, F.; Zhang, C.; Wang, Y.; Yang, J.; Kang, S.; Shen, K. Genetic models and exploration implication of the paleochannel sandstone-type uranium deposits in the Erlian Basin, North China–A review and comparative study. *Ore Geol. Rev.* **2020**, *127*, 103821. [CrossRef]
58. Nie, F.J.; Yan, Z.B.; Xia, F.; He, J.F.; Zhang, C.Y.; Feng, Z.B.; Zhang, X.; Yang, D.G.; Chen, M.Y.; Tan, S.J.; et al. Two-stage and Two-mode Uranium Mineralization for Sandstone-type Uranium Deposits. *Acta Geosci. Sin.* **2021**, *42*, 823–848. (In Chinese)
59. Nie, F.J.; Yang, S.Q.; Feng, Z.B.; Xia, F.; Luo, M.; Wang, S.Y.; Zhang, B.C. Constraints of Uplift on Sandstone-type Uranium Mineralization and Its Implications for Prospecting. *Acta Geosci. Sin.* **2024**, *45*, 265–277. (In Chinese)
60. Feng, Z.B.; Nie, F.J.; Ning, Y.L.; Jiang, L.; Xia, F.; He, J.F.; Sheng, Z.N. Discussion and design of exploration technology for sandstone-type uranium deposits in the interior of the sedimentary basins. *Acta Geol. Sin.* **2022**, *96*, 2217–2229. (In Chinese)
61. Feng, Z.B.; Nie, F.J.; Xia, F.; Mangen, L.; Li, J.; Hujun, Z.; Zhaobin, Y.; Chengyong, Z.; Xin, Z. Discussion on the Shapes and Their Genesis of Ore Body in Sandstone-type Uranium Deposits. *Uranium Geol.* **2021**, *37*, 981–990. (In Chinese)
62. Liu, X.X.; Zhao, L.J.; Yu, A.R.; Tang, C. Rock geochemistry characteristics and geological significance of sandstone-type uranium deposits in Luhai area, Erlian Basin. *N. China Geol.* **2024**, *47*, 36–45. (In Chinese)
63. Luo, N.; Chen, L.L.; Yu, A.R.; Li, J.M.; Zang, Y.L.; Yu, X.L.; Liu, Y. Metallogenic Geologic Condition of Beiciwa Sandstone-hosted Uranium Deposit in Naomugen Depression, Central Erlian Basin. *J. Henan Polytech. Univ. Nat. Sci. Ed.* **2025**, 1–13. (In Chinese) [CrossRef]
64. Li, T.; Yu, A.R.; Yang, T.X.; Si, Q.H.; Zhu, Q.; Peng, S.L. Geological characteristics and prospecting factors of sandstone type uranium deposits in Baiyanhua area, Western Erlian Basin. *N. China Geol.* **2022**, *45*, 38–47, 74. (In Chinese)
65. Thompson, A.J.B.; Hauff, P.L.; Robitaille, A.J. Alteration Mapping in Exploration: Application of Short-Wave Infrared (SWIR) Spectroscopy. *SEG Discov.* **1999**, 1–27. [CrossRef]
66. Hapke, B. *Theory of Reflectance and Emittance Spectroscopy*; Cambridge University Press: Cambridge, UK, 2012.
67. Clark, R.N. Spectroscopy of rocks and minerals, and principles of spectroscopy. In *Remote Sensing for the Earth Sciences Manual of Remote Sensing*; John Wiley & Sons: Hoboken, NJ, USA, 1999; Volume 3.
68. Liu, L.H.; Zhang, P.P.; Li, X.Z. FTIR Analysis of Metallic Sulfide Minerals. *Anal. Test. Technol. Instrum.* **2006**, *12*, 34–37. (In Chinese)
69. Jones, S.; Herrmann, W.; Gemmell, J.B. Short Wavelength Infrared Spectral Characteristics of the HW Horizon: Implications for Exploration in the Myra Falls Volcanic-Hosted Massive Sulfide Camp, Vancouver Island, British Columbia, Canada. *Econ. Geol.* **2005**, *100*, 273–294. [CrossRef]
70. Lian, C.Y.; Zhang, G.; Yuan, C.H. Application of SWIR reflectance spectroscopy to Pulang porphyry copper ore district, Yunnan Province. *Miner. Depos.* **2005**, *24*, 621–637. (In Chinese)
71. Lian, C.Y.; Zhang, G.; Yuan, C.H.; Yang, K. Application of SWIR reflectance spectroscopy in mapping of hydrothermal alteration minerals: A case study of the Tuwu porphyry copper prospect, Xinjiang. *Geol. China* **2005**, *32*, 483–495. (In Chinese)
72. Zhang, G.; Lian, C.Y.; Wang, R.S. Application of the portable infrared mineral analyser (PIMA) in mineral mapping in the Qulong copper prospect, Mozhugongka County, Tibet. *Geol. Bull. China* **2005**, *24*, 480–484. (In Chinese)
73. Laakso, K.; Peter, J.M.; Rivard, B.; White, H.P. Short-Wave Infrared Spectral and Geochemical Characteristics of Hydrothermal Alteration at the Archean Izok Lake Zn-Cu-Pb-Ag Volcanogenic Massive Sulfide Deposit, Nunavut, Canada: Application in Exploration Target Vectoring. *Econ. Geol.* **2016**, *111*, 1223–1239. [CrossRef]
74. Zinsser, A. Hydrothermal alteration in the Yellow Pine deposit, stibnite gold project, Idaho; Vein cross cutting, VIR-NIR-SWIR spectroscopy and multi-element geochemistry. In Proceedings of the 68th Annual Meeting, Geological Society of America (GSA) Rocky Mountain Section, Moscow, ID, USA, 18–19 May 2016.
75. Xu, C.; Chen, H.Y.; White, N.; Qi, J.P.; Zhang, L.J.; Zhang, S.; Duan, G. Alteration and mineralization of Xinan Cu-Mo ore deposit in Zijinshan orefield, Fujian Province, and application of short wavelength infra-red technology (SWIR) to exploration. *Miner. Depos.* **2017**, *36*, 1013–1038. (In Chinese)
76. Zhang, C.; Ye, F.W.; Yao, J.L.; Che, Y.F.; Tian, M.J. Implementation method of drill core logging based on imaging spectrometer. *Remote Sens. Inf.* **2017**, *32*, 69–74. (In Chinese)
77. Guo, N.; Shi, W.; Huang, Y.; Zheng, L.; Tang, N.; Wang, C.; Fu, Y. Alteration mapping and prospecting model construction in the Tiegelongnan ore deposit of the Duolong ore concentration area, northern Tibet, based on shortwave infrared technique. *Geol. Bull. China* **2018**, *37*, 446–457.

78. Han, J.; Chu, G.; Chen, H.; Hollings, P.; Sun, S.; Chen, M. Hydrothermal alteration and short wavelength infrared (SWIR) characteristics of the Tongshankou porphyry-skarn Cu-Mo deposit, Yangtze craton, Eastern China. *Ore Geol. Rev.* **2018**, *101*, 143–164. [CrossRef]
79. Huang, J.; Chen, H.; Han, J.; Deng, X.; Lu, W.; Zhu, R. Alteration zonation and short wavelength infrared (SWIR) characteristics of the Honghai VMS Cu-Zn deposit, Eastern Tianshan, NW China. *Ore Geol. Rev.* **2018**, *100*, 263–279. [CrossRef]
80. Jing, X.K. Application of Short Wave Infrared (SWIR) Technique in Exploration of Dongshibu in Tibet. Master's Thesis, China University of Geosciences, Beijing, China, 2018. (In Chinese)
81. Sun, L.; Khan, S.; Shabestari, P. Integrated Hyperspectral and Geochemical Study of Sediment-Hosted Disseminated Gold at the Goldstrike District, Utah. *Remote Sens.* **2019**, *11*, 1987. [CrossRef]
82. Tian, J.; Zhang, Y.; Cheng, J.-M.; Sun, S.-Q.; Zhao, Y.-J. Short wavelength infra-red (SWIR) characteristics of hydrothermal alteration minerals in skarn deposits: Example from the Jiguanzui Cu–Au deposit, Eastern China. *Ore Geol. Rev.* **2019**, *106*, 134–149. [CrossRef]
83. Guo, N.; Guo, W.; Shi, W.; Huang, Y.; Guo, Y.; Lian, D. Characterization of Illite Clays associated with the Sinongduo low sulfidation epithermal deposit, Central Tibet using field SWIR spectrometry. *Ore Geol. Rev.* **2020**, *120*, 103228. [CrossRef]
84. Zhang, S.; Chu, G.; Cheng, J.; Zhang, Y.; Tian, J.; Li, J.; Sun, S.; Wei, K. Short wavelength infrared (SWIR) spectroscopy of phyllosilicate minerals from the Tonglushan Cu-Au-Fe deposit, Eastern China: New exploration indicators for concealed skarn orebodies. *Ore Geol. Rev.* **2020**, *122*, 103516. [CrossRef]
85. Zhou, Y.; Chen, S.; Li, L.; Fan, F.; Zhang, H.; Chen, J.; Yang, K.; Xiu, L.; Xu, M.; Xing, G. Mapping hydrothermal alteration of the Au-Cu deposits in the Zhenghe magmatic-hydrothermal mineralization system, SE China, using Short Wavelength Infrared (SWIR) reflectance spectroscopy. *J. Geochem. Explor.* **2023**, *244*, 107113. [CrossRef]
86. Zhou, Y.; Li, L.; Yang, K.; Xing, G.; Xiao, W.; Zhang, H.; Xiu, L.; Yao, Z.; Xie, Z. Hydrothermal alteration characteristics of the Chating Cu-Au deposit in Xuancheng City, Anhui Province, China: Significance of sericite alteration for Cu-Au exploration. *Ore Geol. Rev.* **2020**, *127*, 103844. [CrossRef]
87. Hiatt, E. Fluids in sedimentary basins: An introduction. *J. Geochem. Explor.* **2003**, *80*, 139–149. [CrossRef]
88. Wang, C.W.; Guo, N.; Guo, K.; Zhang, T.T. Characteristics of the Chlorite Alteration in the Porphyry-Skarn Deposit Based on Short-Wave Infrared Technology: A Case Study of the Jiama Copper-Polymetallic Deposit in Tibet. *Geol. Explor.* **2014**, *50*, 1137–1146. (In Chinese)
89. Wang, L.; Percival, J.B.; Hedenquist, J.W.; Hattori, K.; Qin, K. Alteration Mineralogy of the Zhengguang Epithermal Au-Zn Deposit, Northeast China: Interpretation of Shortwave Infrared Analyses During Mineral Exploration and Assessment. *Econ. Geol.* **2021**, *116*, 389–406. [CrossRef]
90. Wang, X.H.; Duan, S.G.; Sun, P.; Zhai, S.D.; Zhang, Y. Short-wave infrared spectroscopy analysis and prospecting indication of hydro^{-} thermal alteration of Waigang silver polymetallic deposit in Zhejiang, China. *Miner. Depos.* **2022**, *41*, 174–188. (In Chinese)
91. Yang, X.Y.; Ling, M.X.; Sun, W.; Miao, J.Y.; Liu, C.Y. Characteristics of fluid inclusions in sandstone-type uranium deposit of Ordos Basin. *Acta Pet. Sin.* **2006**, *27*, 28–33. (In Chinese)
92. Richard, A.; Rozsypal, C.; Mercadier, J.; Banks, D.A.; Cuney, M.; Boiron, M.; Cathelineau, M. Giant uranium deposits formed from exceptionally uranium rich acidic brines. *Nat. Geosci.* **2012**, *5*, 142–146. [CrossRef]
93. Ghoneim, M.M.; Panova, E.G.; Abdel Gawad, A.E. Natural radioactivity and geochemical aspects of radioactive mineralisation in El Sela, South Eastern Desert, Egypt. *Int. J. Environ. Anal. Chem.* **2023**, *103*, 2338–2350. [CrossRef]